ACS OMEGA

http://pubs.acs.org/journal/acsodf

Article

Development and Evaluation of Some Molecular Hybrids of *N*-(1-Benzylpiperidin-4-yl)-2-((5-phenyl-1,3,4-oxadiazol-2-yl)thio) as Multifunctional Agents to Combat Alzheimer's Disease

Digambar Kumar Waiker, Akash Verma, Poorvi Saraf, Gajendra T.A., Sairam Krishnamurthy, Rameshwar Nath Chaurasia, and Sushant Kumar Shrivastava*

Cite This: *ACS Omega* 2023, 8, 9394−9414

Read Online

ACCESS | Metrics & More | Article Recommendations | Supporting Information

ABSTRACT: A series of some novel compounds (**SD-1**−**17**) were designed following a molecular hybridization approach, synthesized, and biologically tested for hAChE, hBChE, hBACE-1, and Aβ aggregation inhibition potential to improve cognition and memory functions associated with Alzheimer's disease. Compounds **SD-4** and **SD-6** have shown multifunctional inhibitory profiles against hAChE, hBChE, and hBACE-1 enzymes *in vitro*. Compounds **SD-4** and **SD-6** have also shown anti-Aβ aggregation potential in self- and acetylcholinesterase (AChE)-induced thioflavin T assay. Both compounds have shown a significant propidium iodide (PI) displacement from the cholinesterase-peripheral active site (ChE-PAS) region with excellent blood−brain barrier (BBB) permeability and devoid of neurotoxic liabilities. Compound **SD-6** ameliorates cognition and memory functions in scopolamine- and Aβ-induced behavioral rat models of Alzheimer's disease (AD). *Ex vivo* biochemical estimation revealed a significant decrease in malonaldehyde (MDA) and AChE levels, while a substantial increase of superoxide dismutase (SOD), catalase, glutathione (GSH), and ACh levels is seen in the hippocampal brain homogenates. The histopathological examination of brain slices also revealed no sign of neuronal or any tissue damage in the **SD-6**-treated experimental animals. The *in silico* molecular docking results of compounds **SD-4** and **SD-6** showed their binding with hChE-catalytic anionic site (CAS), PAS, and the catalytic dyad residues of the hBACE-1 enzymes. A 100 ns molecular dynamic simulation study of both compounds with ChE and hBACE-1 enzymes also confirmed the ligand−protein complex's stability, while quikprop analysis suggested drug-like properties of the compounds.

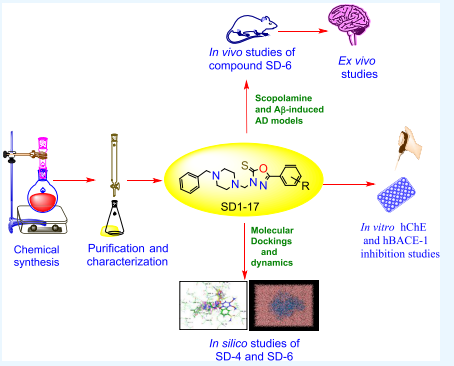

1. INTRODUCTION

Alzheimer's disease (AD) is the most common form of dementia and is often linked to memory impairment and decline in cognitive functions in people over the age of 60.[1,2] According to the World Alzheimer's Report 2021, 55 million people are positive dementia survivors, and this figure is expected to grow up to 78 million by 2030. It is also estimated that more than 75% of people with dementia are living without diagnosis and this figure may even be higher as up to 90% in low- and middle-income countries due to a lack of awareness.[3] AD may contribute 60−70% of total dementia cases, which is expected to be 152 million globally by 2050.[4] The existing AD therapies only provide symptomatic relief without halting its progression, thus imposing a socioeconomic burden on middle-income countries.[5] AD before the age of 60 is known as familial AD (FAD) and is often associated with different gene mutations such as presenilins (PSEN1 and PSEN2 genes) and amyloid precursor protein (APP), which accounts for less than 1% of the AD patient.[6,7] Another form of AD that appears in people over the age group of 65 years, known as sporadic AD (SAD), is associated with several factors such as apolipoprotein E (APOE) that is believed to be the most common for SAD and late onset of FAD.[8,9]

The exact cause and treatment of AD are still in their infancy owing to the multifaceted pathophysiology involved in the disease and its progression. Several factors such as lower acetylcholine (ACh) levels,[10] increased acetylcholinesterase (AChE) in the synaptic cleft,[11] activation of *N*-methyl-D-aspartate receptor (NMDAR),[12] central nervous system (CNS) inflammation in response to activated microglial cells and astrocytes,[13] hyperphosphorylated tau and formation of neurofibrillary tangles (NFTs),[14] oxidative stress,[15] and accumulation of amyloid β (Aβ) and its aggregates[10] are the hallmarks of AD and its progression.

Received: December 19, 2022
Accepted: February 22, 2023
Published: March 2, 2023

https://doi.org/10.1021/acsomega.2c08061
ACS Omega 2023, 8, 9394−9414

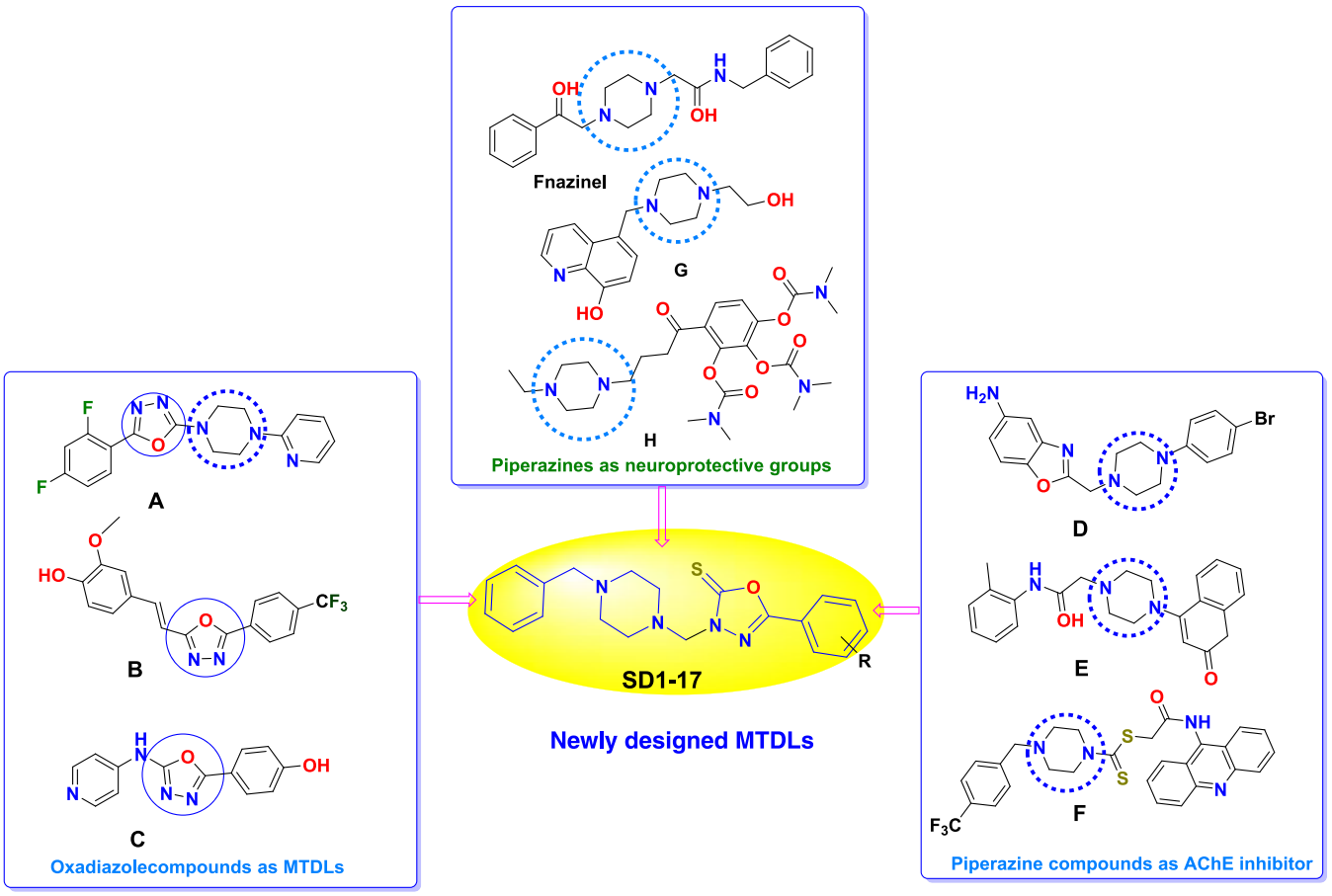

Figure 1. Designing strategy of the present series of compounds **SD-1−17** using the molecular hybridization approach.

Widespread efforts are continuously being made in search of the drug for AD.[16] The current treatment regimen for AD therapy involves the use of NMDA receptor antagonist (memantine) and AChE inhibitors (donepezil, rivastigmine, and galantamine) that deliver symptomatic relief with slight cognition and memory improvements in AD.[17] Recently, aducanumab (monoclonal antibody) has been approved by Food and Drug Administration (FDA) as a disease-modifying therapy for AD. Aducanumab is associated with improvements in memory and cognitive impairments linked to Aβ plaques, though its use is still controversial in AD progression.[18]

Several mechanisms and hypotheses have been proposed explaining the progression of AD. However, a precise etiology is still elusive.[19] Several hypotheses govern AD progression, among which cholinergic transmission dysfunction and formation of Aβ-aggregates have emerged as the widely acceptable pathophysiology for synaptic loss and neurodegeneration.[20,21] The cholinesterase enzymes (ChEs), *i.e.*, AChE and butyrylcholine esterase (BChE) inhibitors, are the most promising therapeutic strategy to halt proteolytic degradation of the ACh into choline and acetic acid and increase ACh levels in synaptic cleft to regulate cholinergic neurotransmission.[22] AChE and BChE were also observed to promote Aβ-aggregation and the formation of neocortical Aβ-plaques and neurofibrillary tangles.[23] Another most widely acceptable cause of AD is Aβ-aggregation, which results in synaptic loss and, ultimately, neuronal cell death. Aβ accumulates in the brain as an insoluble protein in response to β secretase-1 (BACE-1)-associated APP cleavage. The accumulation of Aβ results in neuroinflammation and also elevates free-radical production in the mitochondria of the neuronal cell causing oxidative stress.[24]

Therefore, designing an inhibitor that could intervene multiple targets at a time to restore impaired learning and memory functions (ChE inhibition) along with the capabilities to reduce Aβ-aggregation and neuroinflammation (BACE-1 inhibition) would be a promising candidate to stop progression rather than providing symptomatic relief to AD sufferers. In the present work, a multitarget-directed ligand (MTDL)-based approach was utilized to design novel molecular hybrids with anti-hAChE, hBChE, hBACE-1, and Aβ-aggregation capabilities where a series of 17 molecular hybrids were successfully designed, synthesized, and tested for their *in vitro* inhibitory potentials of interest. The binding of the compound to the AChE-peripheral active site (PAS) was examined by propidium iodide (PI) displacement assay. The potent compounds from the series have been further tested for their blood−brain barrier (BBB) capabilities by peripheral artificial membrane permeability assay (PAMPA−BBB assay). The neurotoxicity and neuroprotective estimation of the potent compounds were performed on differentiated and nondifferentiated SH-SY5Y cell lines, respectively. The type of inhibition of the most active compound was performed by enzyme kinetics study. The most potent compound was also estimated *in vivo* (Y-maze and Aβ-induced Morris water maze test) for behavioral improvements in the experimental animals (rat model). The *ex vivo* estimation of various biochemical markers was also determined in the brain (hippocampal) homogenate of the experimental

https://doi.org/10.1021/acsomega.2c08061
ACS Omega 2023, 8, 9394−9414

Scheme 1. Synthesis of Targeted Compounds SD-1−17[a]

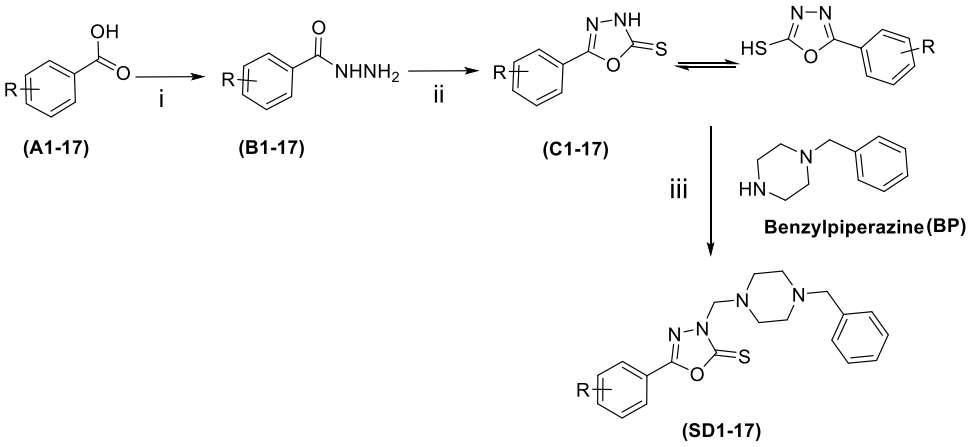

[a]Reagents and conditions: (i) HOBT, EDC·HCl, acetonitrile, $NH_2NH_2{\cdot}2H_2O$, 0−5 °C, 2 h, 78−91%; (ii) CS_2, KOH, ethanol, reflux, 3 h, 85−89%; and (iii) HCHO, ethanol, RT, 16 h, 58−78%.

animals. The brain tissue histopathology (hippocampal brain) of the animals (Aβ-induced) treated with the most potent compound and the standard drug was also estimated to evaluate the neuronal cell morphology and density.

2. RESULTS AND DISCUSSION

2.1. Designing Strategy. The real cause of AD is still mysterious, and it is considered that multifaceted pathophysiology is involved in the development and progression of the disease. A novel series of compounds **SD-1−17** were designed using an MTDL approach utilizing molecular hybridization methodology based on the previously reported compounds from our laboratory, *i.e.*, **A** (hAChE; IC_{50} = 0.054 ± 0.002 μM, hBChE; IC_{50} = 0.787 ± 0.022 μM and hBACE-1; IC_{50} = 0.098 ± 0.004 μM), **B** (hAChE; IC_{50} = 0.055 ± 0.003 μM, hBChE; IC_{50} = 0.186 ± 0.005 μM and hBACE-1; IC_{50} = 0.146 ± 0.012 μM), and **C** (hAChE; pIC_{50} = 6.52 ± 0.04 μM, hBChE; pIC_{50} = 4.92 ± 0.05 μM with antioxidant activity) containing 5-phenyl-1,3,4-oxadiazole scaffold, which has shown good MTDL capabilities.[25−27] Other compounds **D** (eeAChE; IC_{50} = 0.052 ± 0.010 μM, eeBChE; IC_{50} = 1.085 ± 0.035 μM), **E** (IC_{50} = 8.3 ± 0.04 μM), and **F** (63−68% inhibition) having a piperazine ring present on it have shown good inhibitory results against AChE.[28−32] Compounds **G** and **H**, also containing a piperazine moiety, have demonstrated neuroprotective activity, while the fenazinel (NMDAR antagonist against ischemic stroke) has also exhibited neuroprotective activity owing to its piperazine moiety.[29,33,34]

To design a new molecular hybrid, 5-phenyl-1,3,4-oxadiazole was selected as a lead scaffold (Figure 1) due to its binding in the AChE-PAS region, which was replaced with substituted 5-phenyl-1,3,4-oxadiazole-2-thione. The sulfur atom was introduced in the scaffold as it has an established role in improving the defense mechanism against oxidative stress and reactive oxygen species (ROS) in pathological diseased conditions.[35] The benzylpiperazine (BP) moiety was attached to 3-NH of 1,3,4-oxadiazole-2-thione through a single carbon chain linker with an assumption that it will provide enough flexibility and optimum length to the BP ring to accommodate the AChE-catalytic anionic site (CAS) and catalytic dyad (Asp32 and Asp228 residues) of the BACE-1 enzyme, respectively. The BP moiety was also introduced owing to the protonation capabilities of its nitrogen atom at the physiological pH that will lead to enhanced BBB permeability, ChE, and BACE-1 inhibitory activity.[26] Various electron-withdrawing groups (EWGs) and electron-donating groups (EDGs) were attached to the 5-phenyl ring to generate a structure−activity relationship (SAR) of the designed compounds against ChE and BACE-1 enzymes.

2.2. Chemistry. Synthesis of the designed compounds **SD-1−17** was achieved by following a three- to four-step protocol depicted in Scheme 1. Benzoic acids (**A1−17**) were used as the starting materials for the reaction and reacted with *N*-hydroxybenzotriazole (HOBT) in the presence of 1-ethyl-3-(3-dimethylaminopropyl)carbodiimide (EDC) in acetonitrile (ACN) to produce the corresponding benzoic acid esters. These esters were then subsequently reacted *in situ* with hydrazine hydrate at ice-cold (0−5 °C) to room-temperature (RT) conditions producing the corresponding benzohydrazide (**B1−17**). The formation of intermediates (**B1−17**) was initially confirmed by Fourier-transform infrared (FT-IR) spectroscopy, which showed the presence of two stretching bands of −NH at 3260−3135 and 3147−3078 cm^{-1} and a single stretching band of $-NH_2$ between 3426 and 3340 cm^{-1}. The structure of the intermediates (**B1−17**) was also confirmed by ^{1}H NMR, which showed the presence of one −NH proton around 10−9 ppm and two $-NH_2$ protons at 5−4 ppm. The intermediates (**B1−17**) were further reacted with carbon disulfide (CS_2) under a basic environment (KOH) in dimethylformamide (DMF) to obtain secondary intermediates (**C1−17**), the FT-IR spectra of which demonstrated the presence of the C═S stretching band at 1270−1220 cm^{-1}. The chemical structure of the intermediates was further validated by ^{1}H NMR spectroscopy, which showed the presence of −SH proton at 12−11 ppm. The final compounds **SD-1−17** were prepared using the Mannich reaction where secondary intermediates (**C1−17**) in hot ethanolic solution were reacted with formaldehyde (HCHO) and BP. The structure of the final compounds was confirmed by the FT-IR, which showed the presence of C═S at 1270−1220 cm^{-1} and methylene ($-CH_2$) group at 2950−2850 cm^{-1}. The secondary intermediates (**C1−17**) exist in −SH and −C═S tautomeric forms, which finally convert into −C═S after losing an acidic proton from the 3-NH of the 1,3,4-oxadiazole-2-thiol ring. The ^{1}H NMR spectra of the compounds have also shown the presence of two $-CH_2$ protons between 5 and 3 ppm. The

https://doi.org/10.1021/acsomega.2c08061
ACS Omega 2023, 8, 9394−9414

Table 1. *In Vitro* ChE and hBACE-1 Inhibitory Activity of the Synthesized Compounds

		$IC_{50} \pm SEM$ (μM)[b]			
compound code	R	hAChE	hBChE	hBACE-1	selectivity index[c] hBChE/hAChE
SD-1	4-Cl	1.255 ± 0.019	>10	0.943 ± 0.018	nd[a]
SD-2	4-NO_2	1.107 ± 0.008	>10	0.811 ± 0.023	nd
SD-3	4-OCF_3	1.335 ± 0.012	>10	1.113 ± 0.016	nd
SD-4	3-CN	1.077 ± 0.009	1.653 ± 0.019	0.651 ± 0.014	1.534
SD-5	2-NO_2	1.885 ± 0.031	>10	1.172 ± 0.021	nd
SD-6	H	0.907 ± 0.011	1.579 ± 0.037	0.753 ± 0.018	1.703
SD-7	3-Cl	1.424 ± 0.022	>10	0.885 ± 0.013	nd
SD-8	4-CF_3	1.316 ± 0.018	2.416 ± 0.041	0.701 ± 0.019	1.835
SD-9	2,4-di Cl	2.115 ± 0.037	>10	1.414 ± 0.031	nd
SD-10	4-OH	1.224 ± 0.013	>10	>5	nd
SD-11	4-NH_2	1.218 ± 0.027	>10	>5	nd
SD-12	3-OCH_3	1.937 ± 0.024	>10	1.214 ± 0.016	nd
SD-13	4-OCH_3	1.531 ± 0.028	>10	1.358 ± 0.012	nd
SD-14	4-Cl, 3-NO_2	1.136 ± 0.018	1.943 ± 0.033	0.806 ± 0.011	1.710
SD-15	2,4-di NO_2	1.419 ± 0.023	>10	1.447 ± 0.022	nd
SD-16	2-Br	2.408 ± 0.027	>10	1.801 ± 0.029	nd
SD-17	2,4-di OH	1.792 ± 0.015	>10	2.154 ± 0.034	nd
donepezil		0.054 ± 0.006	2.557 ± 0.038	1.413 ± 0.017	47.351
rivastigmine		1.701 ± 0.024	1.312 ± 0.013	nd	0.771

[a]nd, the *in vitro* activity or selectivity of the compounds not performed. [b]The *in vitro* activity of the compounds is represented as IC_{50} ± standard error of the mean (SEM) of three individual experiments (n = 3). [c]Selectivity index for hAChE = IC_{50} of hBChE/IC_{50} of hAChE; hAChE inhibition—good (≤1.0 μM), moderate (between 1.0 and 2.0 μM), and poor (>2.0 μM); hBChE inhibition—good (≤1.5.0 μM), moderate (between 1.5 and 2.5 μM), and poor (>3 μM); hBACE-1 inhibition—good (1.5.0 μM), moderate (between 1.5 and 2.5 μM), and poor (>2.5 μM).

structure of the final compounds (**SD-1−17**) was confirmed by the ^{13}C NMR spectra, which have shown the presence of two carbon signals of methylene (−CH_2) around 70−60 ppm and two piperazine carbon signals at 60−50 ppm. The percentage purity of the final compounds was also estimated through the high-performance liquid chromatography (HPLC), which showed purity >95%. The high-resolution mass spectrometry (HRMS) spectra of the final compounds have also demonstrated the presence of the corresponding masses.

2.3. Pharmacology. *2.3.1. In Vitro Cholinesterase (hAChE and hBChE) Inhibition Assay.* The *in vitro* inhibitory potential of the compounds (**SD-1−17**) was estimated using Ellman's colorimetric method. Most of the synthesized compounds have shown good to moderate, while a few showed poor hAChE inhibitory activity. The representative compound of the series **SD-6** that contains an unsubstituted phenyl ring on 1.3.4-oxadiazole-2-thione showed good hAChE inhibitory (IC_{50} = 0.907 ± 0.011 μM) activity as compared to rest of the molecules of the series. As described in Table 1, the compounds like **SD-1** (Cl), **SD-2** (−NO_2), **SD-3** (−OCF_3), **SD-8** (−CF_3), **SD-10** (−OH), and **SD-11** (−NH_2) containing an EWG at the fourth position of the phenyl ring have shown moderate hAChE inhibitory activity. The introduction of EWG at the third position of the phenyl ring as in compounds **SD-4** (−C≡N) and **SD-7** (3-Cl) has shown good hAChE inhibition. Among them, the compound containing the 3-C≡N group showed better activity than the 3-Cl group compound. The introduction of disubstituted EWGs at the phenyl ring of the compounds like **SD-9** (2,4-di Cl), **SD-15** (2,4-di NO_2), and **SD-17** (2,4-di OH) and the substitution of EWG at the second position in compounds **SD-5** (2-NO_2) and **SD-16** (2-Br) have shown moderate to poor hAChE inhibitory activity. However, the 3,4-disubstituted EWG-containing compound **SD-14** (4-Cl, 3-NO_2) and EDG at the third and fourth positions of phenyl rings **SD-12** (3-OCH_3) and **SD-13** (4-OCH_3) have shown moderate hAChE inhibition. Peripheral BChE inhibition could also be a therapeutic strategy for halting AD progression.[36] The dual AChE and BChE inhibition could be advantageous in AD as disease-modifying therapy rather than symptomatic relief.[37] To investigate the dual cholinesterase (ChE) inhibitory profile of the synthesized compounds, an *in vitro* hBChE inhibitory colorimetric assay method was performed. The *in vitro* hBChE assay results (Table 1) showed that compounds **SD-4** and **SD-6** were the representative hBChE inhibitors among the series. Two more compounds **SD-8** and **SD-14** of the series have also demonstrated good hBChE inhibitory potential, while the other compounds of the series were less potent (IC_{50} > 10 μM) against the enzyme. The *in vitro* hAChE and hBChE inhibitory potentials of the compounds (**SD-1−17**) were measured and compared with the standard drugs donepezil (hAChE; IC_{50} = 0.054 ± 0.006 μM and hBChE; IC_{50} = 2.557 ± 0.038 μM) and rivastigmine (hAChE; IC_{50} = 1.701 ± 0.024 μM and hBChE, IC_{50} = 1.312 ± 0.013 μM).

The *in vitro* findings suggested that the unsubstituted phenyl ring at 1.3.4-oxadiazole-2-thione is more favorable for dual hAChE and hBChE inhibition, while substituted EWGs at the 4-position of the phenyl ring have shown moderate hAChE and poor hBChE inhibitory activity (>10 μM) as compared to the unsubstituted compound. The 3-substituted phenyl ring with EWGs may also be favorable for the hAChE and hBChE inhibitory activities. EDGs at the 3- and 4-positions of the phenyl ring have resulted in diminished hAChE and hBChE activities. However, 3,4-disubstituted compounds at the phenyl ring have shown better hAChE and hBChE activities than the 2,4-disubstituted compounds (Table 1).

2.3.2. hAChE Enzyme Kinetics. The enzyme kinetics study of the most active compound **SD-6** against hAChE was performed to examine the type of inhibition. Three different concentrations of compound **SD-6** were tested against six

https://doi.org/10.1021/acsomega.2c08061
ACS Omega 2023, 8, 9394−9414

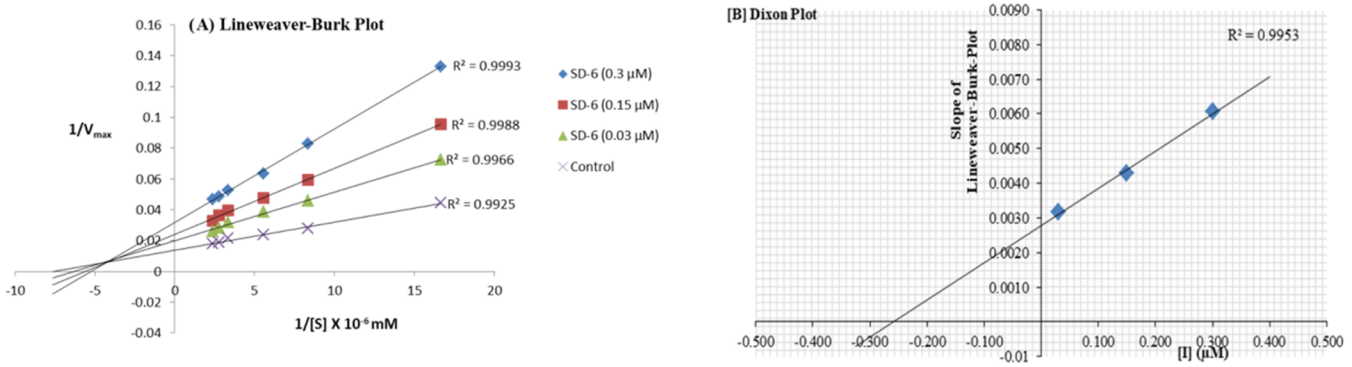

Figure 2. Enzyme kinetics results of compound **SD-6** against hAChE: (A) the Lineweaver–Burk plot showing mixed-type noncompetitive inhibition; (B) Dixon plot showing K_i on the intersecting point of the negative *x*-axis.

Table 2. PI Displacement Assay and PAMPA–BBB Permeability Assay Results of the Compounds[a]

	PAS-AChE propidium iodide displacement (%)[a]		prediction of BBB permeability PAMPA–BBB assay results	
compound	[I] = 10 μM	[I] = 50 μM	$P_{e(exp)}$ (4.8×10^{-6} cm/s)	prediction
SD-4	24.661 ± 1.421	55.157 ± 1.247	6.127 ± 0.019	CNS+[b]
SD-6	27.316 ± 1.208	56.238 ± 1.338	5.643 ± 0.021	CNS+[b]
SD-8	21.446 ± 1.147	41.709 ± 1.271	5.019 ± 0.033	CNS+[b]
SD-14	19.773 ± 1.216	36.841 ± 1.069	4.858 ± 0.016	CNS+[b]
donepezil	23.041 ± 1.019	37.193 ± 1.422	5.264 ± 0.022	CNS+[b]

[a]Displacement of PI from the AChE-PAS region at 10 and 50 μM concentrations. [b]"CNS+" compounds with value $P_e > 4.8 \times 10^{-6}$ cm/s showing excellent BBB permeability. The results of three individual experiments (n = 3) are represented as mean ± SEM.

different concentrations of the substrates (acetylthiocholine iodide (ATCI)) along with a fixed enzyme concentration. The Lineweaver–Burk double reciprocal plot was used to calculate the type of inhibition by plotting the increasing substrate concentration on the *x*-axis and their respective reaction velocities on the *y*-axis. The Lineweaver–Burk plot for compound **SD-6** against hAChE showed a mixed-type noncompetitive inhibition profile (Figure 2A). However, the Lineweaver–Burk plot has also demonstrated increased K_m (Michaelis constant) at increased inhibitory concentrations. The dissociation-constant K_i was also determined for compound **SD-6** using the Dixon plot (Figure 2B), which was constructed by plotting the inhibitor concentration on the *x*-axis and the slope of the Lineweaver–Burk plot on the *y*-axis. The dissociation-constant K_i was calculated as the value of an intersecting point on the negative *x*-axis, which was found to be 0.26. The final experimental value was determined as an average of three individual experiments (n = 3).

2.3.3. In Vitro hBACE-1 Inhibition Assay. The increased Aβ aggregation or its reduced clearance results in senile plaque formation that leads to AD development and its progression.[38] Inhibition of BACE-1 controls the formation of APPβ subunits and reduces the Aβ aggregation through the amyloidogenic pathway.[39,40] An hBACE-1 inhibition analysis was performed using a fluorescence resonance energy-transfer (FRET)-based assay to determine the multifunctional inhibition potential of the synthesized derivatives, which have shown a good to moderate inhibition profile. Compounds **SD-1**, **SD-2**, **SD-4**, **SD-6**, **SD-7**, **SD-8**, and **SD-14** have shown (Table 1) good hBACE-1 inhibitory activity (three-digit nanomolar range) among which compound **SD-4** (IC_{50} = 0.753 ± 0.018) has shown a promising hBACE-1 inhibition, which was better than donepezil (IC_{50} = 1.413 ± 0.017 μM). Compounds **SD-3**, **SD-5**, **SD-9**, **SD-12**, **SD-13**, **SD-15**, **SD-16**, and **SD-17** have exhibited moderate hBACE-1 inhibition (Table 1), while the other compounds of the series **SD-10** and **SD-11** have exhibited diminished BACE-1 inhibitory profile (IC_{50} > 5 μM) (Table 1). The overall structure–activity relationship (SAR) of the compounds (**SD-1–17**) against hAChE, hBChE, and hBACE-1 is represented in Figure S1.

2.3.4. Propidium Iodide Displacement Assay. Propidium iodide (PI) assay is a well-established protocol to estimate the binding of a chemical scaffold to the AChE-PAS site. PI has a high affinity toward the AChE-PAS binding site, and it shows up to 10-fold increase in the fluorescence activity upon interaction with the active site.[41] The enzyme kinetics study of the compound **SD-6** has shown a mixed-type noncompetitive inhibitory profile, which suggested that the compound was interacting with the CAS as well as with the PAS site of the enzyme. To affirm the binding of the compounds in the AChE-PAS region, the PI displacement assay was performed. The four compounds (10 and 50 μM concentrations) were selected for the PI displacement assay owing to their good dual AChE and BChE inhibitory activity. The PI assay results demonstrated that both compounds **SD-4** (10 μM: 24.6% and 50 μM: 55.1%) and **SD-6** (10 μM: 27.3% and 50 μM: 56.2%) have significantly displaced the PI as compared to the standard donepezil (10 μM: 23% and 50 μM: 37.1%), while compounds **SD-08** (10 μM: 21.4% and 50 μM: 41.7%) and **SD-14** (10 μM: 19.7% and 50 μM: 36.8%) have comparable PI displacement properties to that of the donepezil (Table 2).

2.3.5. PAMPA–BBB Assay. The blood–brain barrier (BBB) is a dynamic interface membrane that allows only selective biomolecules, chemicals, and ions; meanwhile, it also restricts the entry of toxic chemicals and pathogens into neuronal compartments.[42] The prime requisite for any of the drug molecules to treat brain disorders is to be able to be partitioned across the BBB. To examine the capability of the compounds under investigation to cross BBB, an *in vitro* PAMPA–BBB assay was performed as per the reported

https://doi.org/10.1021/acsomega.2c08061
ACS Omega 2023, 8, 9394–9414

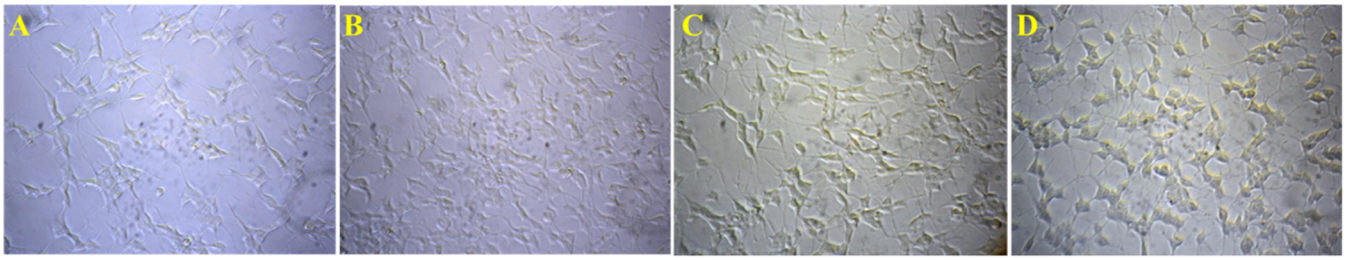

Figure 3. Morphological estimation of the neurotoxicity profile of compounds **SD-4** and **SD-6** in RA/BDNF-differentiated SH-SY5Y cells. (A) Differentiated SH-SY5Y cells alone; (B) cell morphology after incubation with compound **SD-4** (40 μM) for 24 h; (C) cell morphology after incubation with compound **SD-6** (40 μM) for 24 h; and (D) cell morphology after incubation with donepezil (40 μM) for 24 h. The images were captured through phase contrast microscopy.

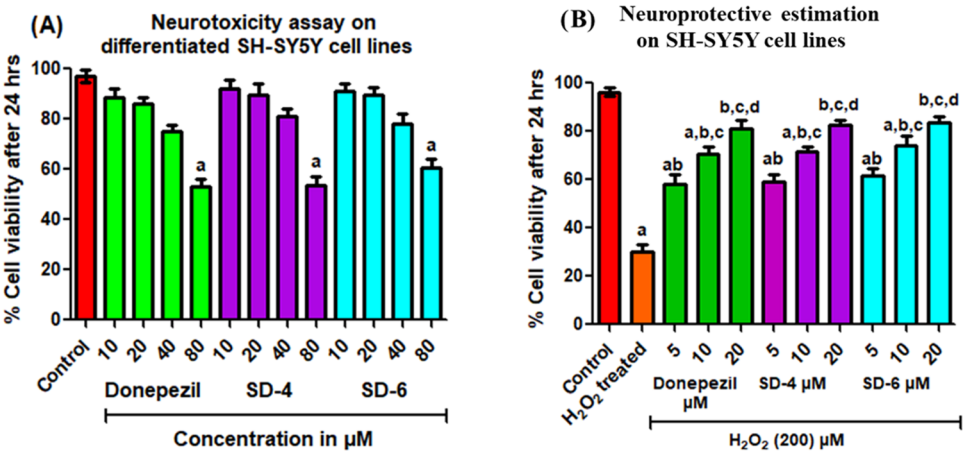

Figure 4. Neurotoxicity and neuroprotective estimation of compounds **SD-4** and **SD-6**; (A) cytotoxicity estimation of compounds **SD-4** and **SD-6** along with donepezil on differentiated SH-SY5Y cell lines. (B) Neuroprotective estimation of **SD-4**, **SD-6**, and donepezil on nondifferentiated SH-SY5Y cell lines in the presence of H_2O_2 (200 μM). ($^{a}p < 0.01$) compared to the control. ($^{a,b}p < 0.05$) ($^{a,b,c}p < 0.01$) ($^{b,c,d}p < 0.001$) compared to H_2O_2-treated.

method.[43] The experimental protocol was validated with seven commercially available drugs with reported BBB permeability as a positive and negative control. A linear correlation graph was plotted between the BBB permeability values obtained for the seven commercially available drugs, and the limit of permeability was defined based on the linear correlation values. The $P_{e(exp)} > 4.8 \times 10^{-6}$ cm/s was selected as the significant value to cross BBB, while the $P_{e(exp)} < 4.8-1.5 \times 10^{-6}$ cm/s was decided as uncertain BBB properties based on the experiments with the positive and negative controls. The PAMPA−BBB assay result demonstrated that all compounds **SD-4** (6.127×10^{-6} cm/s), **SD-6** (5.643×10^{-6} cm/s), **SD-8** (5.019×10^{-6} cm/s), and **SD-14** (4.848×10^{-6} cm/s) had excellent BBB permeability (Table 2). Based on the results of PI displacement and PAMPA−BBB assay compounds, **SD-4** and **SD-06** can further be evaluated as potential leads for other pharmacological investigations.

2.3.6. Neurotoxicity Estimation on Retinoic Acid (RA)/BDNF-Differentiated SH-SY5Y Cell Lines. To investigate the neurotoxic liabilities of compounds **SD-4** and **SD-6** against the neuronal cells, a 3-(4,5-dimethylthiazol-2-yl)-2,5-diphenyl-2*H*-tetrazolium bromide (MTT)-based neurotoxicity assay was performed on retinoic acid (RA) and brain-derived neurotrophic factor (BDNF)-induced differentiated SH-SY5Y cell lines. The SH-SY5Y cells upon treatment with RA exhibited neuron-like properties, *i.e.*, enlarged neurite structures and increased axon span as compared to the normal cells, and have also shown neurite connections with neighboring cells.[44] Both compounds **SD-4** and **SD-6** were tested in 10, 20, 40, and 80 μM concentrations and compared with the donepezil at the same concentrations (Figure 4A). The MTT assay results suggested that at a maximal concentration range of 80 μM, there was no noticeable decrease in the differentiated neuroblastoma cell population as compared to donepezil ($p < 0.01$). All of the selected concentrations of both compounds have also shown neither a change in the shape (neuron-like properties) nor in the neuritic connections (Figure 3) of the cells. Therefore, it can be stated that both compounds **SD-4** and **SD-6** under investigation are non-neurotoxic and can be used further for preclinical research.

2.3.7. SH-SY5Y Neuroprotective Estimation. The neuroprotective activity of compounds **SD-4** and **SD-6** was estimated on the SH-SY5Y cell lines. Initially, the cells were treated with different concentrations of both compounds (5, 10, and 20 μM) for 2 h and H_2O_2 (200 μM) was then added to the cells and incubated further for 24 h. The results suggested that the cell viability was increased in a dose-dependent manner for both the compounds, while the cell viability was significantly decreased to 30.02% in untreated (H_2O_2-treated) cells. Compound **SD-4** has shown a cell viability of 59.1% ($p < 0.01$) at 5 μM, 71.62% ($p < 0.001$) for 10 μM, and 82.47% ($p < 0.001$) for 20 μM concentrations. Similarly, compound **SD-6** has also exhibited a cell viability of 61.40% ($p < 0.01$) at 5 μM, 73.95% ($p < 0.001$) for 10 μM, and 83.57% ($p < 0.001$) for 20 μM concentrations. The results of cell viability data of both compounds were compared with the standard donepezil

https://doi.org/10.1021/acsomega.2c08061
ACS Omega 2023, 8, 9394−9414

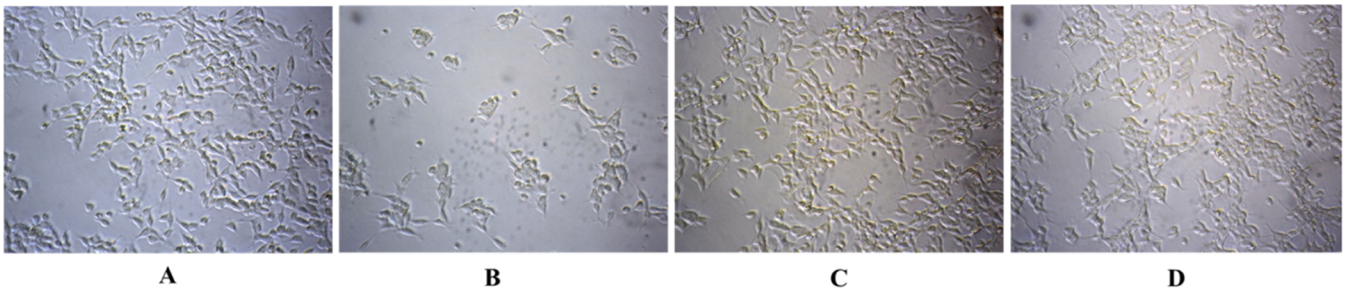

Figure 5. Cell morphology estimation of the neuroprotective activity of compounds **SD-4** and **SD-6** on nondifferentiated SH-SY5Y cells upon cotreatment with H_2O_2. (A) Cells without treatment; (B) cells upon H_2O_2 treatment only; (C) cells treated with **SD-4** (20 μM) in the presence of H_2O_2 (200 μM); and (D) cells treated with **SD-6** (20 μM) in the presence of H_2O_2 (200 μM). The images were captured through phase contrast microscopy.

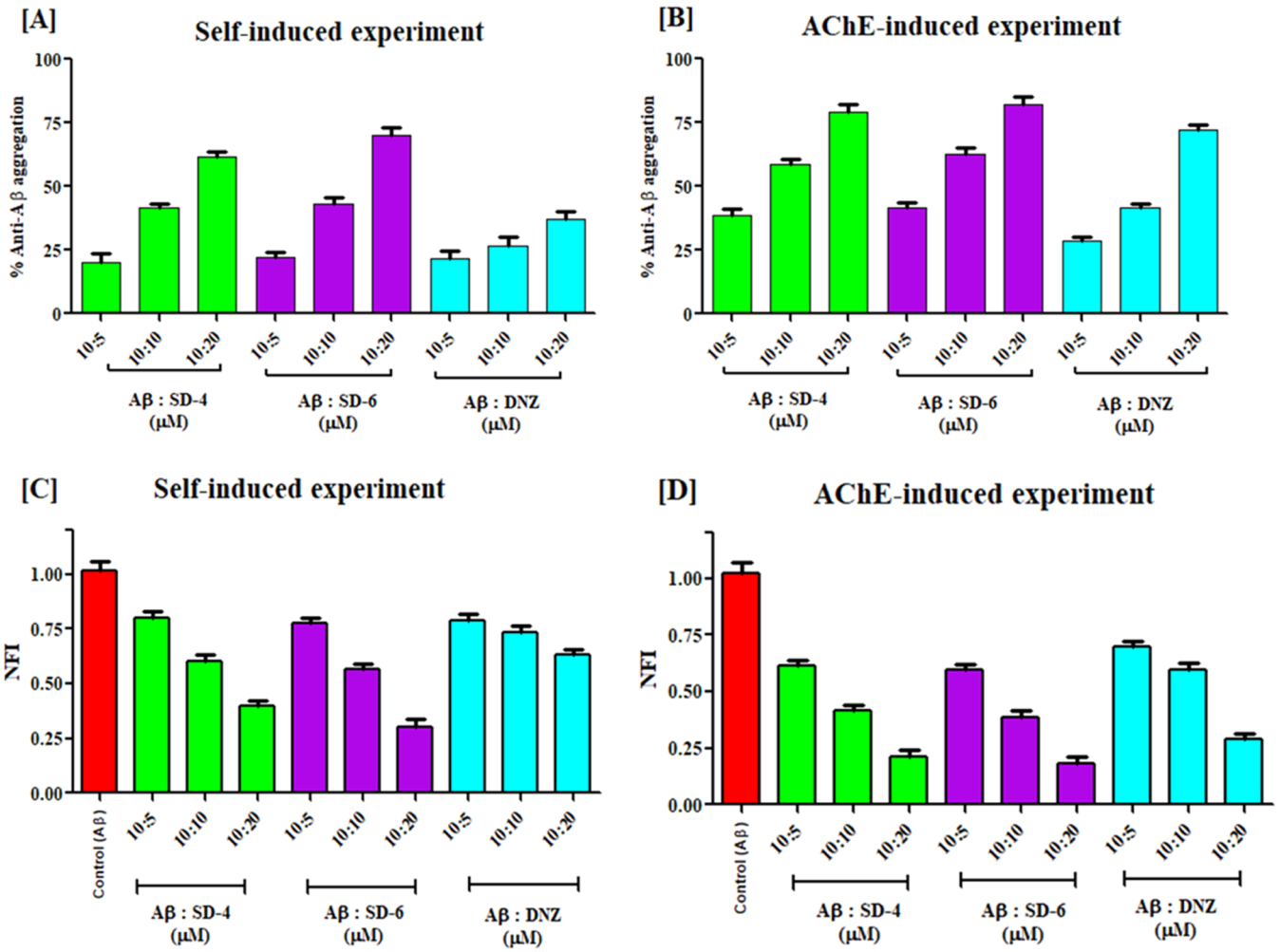

Figure 6. Anti-Aβ aggregation experiments of compounds **SD-4** and **SD-6**: (A) self-induced % anti-Aβ aggregation; (B) AChE-induced % anti-Aβ aggregation; (C) self-induced anti-Aβ aggregation reduced NFI; and (D) AChE-induced anti-Aβ aggregation reduced NFI.

57.92% ($p < 0.01$) at 5 μM, 70.82% ($p < 0.001$) for 10 μM and 81.29% ($p < 0.001$) for 20 μM concentrations, which suggested that both the compounds are equally neuroprotective as donepezil (Figure 4B). The cell morphology was also estimated with and without treatment, which has shown that both compounds have inhibited cell death as compared to cells treated with H_2O_2 (Figure 5).

2.3.8. Aβ-Aggregation Inhibition (Self- and AChE-Induced) Thioflavin T (ThT) Assay. The findings of *in vitro* hAChE inhibition and PI assay indicated that both these compounds could be promising candidates for reducing the Aβ overexpression through an amyloidogenic pathway. Self- and hAChE-induced Aβ experiments were performed using thioflavin T, and the anti-Aβ aggregation potential of compounds **SD-4** and **SD-6** was determined. Three different concentrations (5, 10, and 20 μM) of both compounds were tested against a fixed Aβ concentration (10 μM), and the results are expressed as % Aβ aggregation inhibition and as normalized fluorescence intensity (NFI). ThT experiment has shown that upon incubation of compounds **SD-4** and **SD-6** at

https://doi.org/10.1021/acsomega.2c08061
ACS Omega 2023, 8, 9394−9414

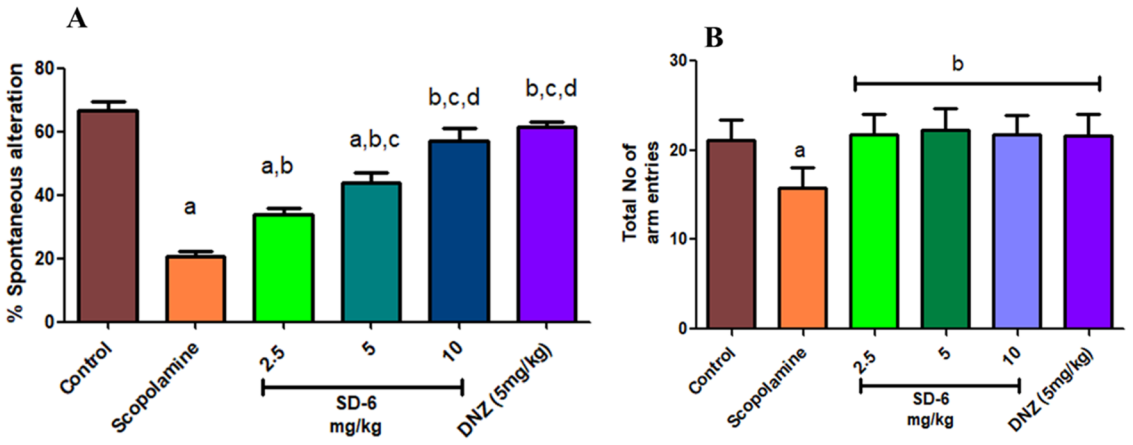

Figure 7. Estimation of **SD-6** and donepezil effects in cognition and memory improvement in scopolamine-induced behavioral models by Y-maze test: (A) % spontaneous alterations and (B) a total number of arm entries. All results are expressed in mean ± SEM ($n = 6$). ($^{a}p < 0.001$) vs control. ($^{a,b}p < 0.05$), ($^{a,b,c}p < 0.01$) and ($^{b,c,d}p < 0.001$) vs scopolamine, ($^{b}p < 0.001$) vs scopolamine.

a 20:10 μM ratio (compound: Aβ) has resulted in reduced fluorescence intensity indicating anti-Aβ aggregation potential of the compounds (Figure S2). The self- and AChE-induced experiments have shown that the anti-Aβ aggregation potential of both compounds **SD-4** and **SD-6** was increased at increasing compound concentrations. Compound **SD-4** (self-induced: 20−61%, hAChE-induced 38−79%) and **SD-6** (self-induced: 22−69%, hAChE-induced 41−81%) have shown slightly higher anti-Aβ aggregation potential as compared to donepezil (self-induced: 21−37%, hAChE-induced 28−72%) (Figure 6A,B). The normalized fluorescence intensity was also calculated for both self- and AChE-induced anti-Aβ aggregation experiments and has shown decreased NFI at increasing compound concentrations (Figure 6C,D), which was better than donepezil at similar concentrations as compared to control (Aβ). Based on our *in vitro* findings, compound **SD-6** was chosen further for *in vivo* investigation.

2.4. *In Vivo* Behavioral Studies. *2.4.1. Acute Toxicity Studies.* Compound **SD-6** was given to healthy nonpregnant female Wistar rats (220−280 g) aged 10−11 weeks to examine the safety profile of the compound. The compound was administered orally following OECD guidelines 423 to the overnight fasted animals in the graduated dose of 100−500 mg/kg, p.o. and was observed for up to 14 days for any abnormal or toxic reactions.[25,45] The results of the acute toxicity study suggested a slight weight loss (12−25%) initially in some animals but regained in 10−12 days in a total 14 day period. Subsequently, the blood samples of the experimental animals were collected and subjected to hepatic and renal function tests, which indicated that all of the associated parameters were within the range (Table S1). After 14 days, the animals were sacrificed and their internal organs such as the kidney, liver, lungs, and heart were examined for any tissue or organ toxicity after H&E staining. The kidney slices have shown normal distal convoluted tubules (DCTs), proximal convoluted tubules (PCTs), and glomerulus, the liver tissue slices have shown normal Kuepfer cells and central vein, while the lung and heart slices have shown normal tissue appearance (Figure S3). The acute toxicity study exhibited that compound **SD-6** was safe and well tolerated by the animals at given doses.

2.4.2. Scopolamine-Induced Y-Maze Test. The scopolamine-induced rat model was used to study the *in vivo* behavioral improvement efficacy of compound **SD-6**. The healthy male Wistar rats (10−11 weeks old and 220−280 g weight) were used in the experiments following i.p. administration of scopolamine (1 mg/kg) to induce cognition and memory deficit functions in animals.[46] Compound **SD-6** was given in three divided doses of 2.5, 5, and 10 mg/kg, p.o., while the standard drug donepezil was given at 5 mg/kg, p.o for 7 days in divided doses. A Y-maze test was performed to determine total arm entries and spontaneous alterations. The animal group treated with scopolamine has shown a significant reduction in % spontaneous alterations ($^{a}p < 0.001$) owing to memory and cognition impairment caused by scopolamine as compared to the control group. The donepezil (5 mg/kg)-treated group has shown a significant ($^{b,c,d}p < 0.001$) increase in % spontaneous alteration as compared to the scopolamine-treated group. However, the animals treated with compound **SD-6** (2.5, 5, and 10 mg/kg) have also shown a significant increase in % spontaneous alterations in a dose-dependent manner (Figure 7A) as compared to the scopolamine-treated group in which 10 mg/kg dose has shown the maximum significant ($^{b,c,d}p < 0.001$) increase in % spontaneous alteration. The results of the Y-maze test have also suggested that the total number of arm entries remained unchanged and were almost equal in each group, showing that scopolamine did not alter the locomotor activity in the experimental animals (Figure 7B).

2.4.3. Aβ-Induced Morris Water Maze Test. The BACE-1 enzyme directly affects the formation and deposition of Aβ *via* an amyloidogenic pathway. BACE-1 propagates Aβ formation through APP cleavage and results in Aβ_{1-42} formation, which affects neuronal cell survival. The effect of compound **SD-6** in a reversal of learning and memory functions in intracerebrovascular (ICV) Aβ_{1-42}-induced male Wistar rat model was evaluated through the Morris water maze test using donepezil as a positive control. The ICV infusion (4 μM, 5 μL) of Aβ_{1-42} in the rat hippocampal region through stereotaxic surgery produces AD-like properties due to microglial activation and neuroinflammation, which leads to memory and cognition deficit and mimics the AD-like behavior.[31] After the ICV infusion of Aβ_{1-42} to each group (except the sham group), both donepezil and compound **SD-6**, 5 and 10 mg/kg, respectively, were administered orally for up to 9 days consecutively to each corresponding group and the only vehicle was administered to the control group (Aβ). The test

https://doi.org/10.1021/acsomega.2c08061
ACS Omega 2023, 8, 9394−9414

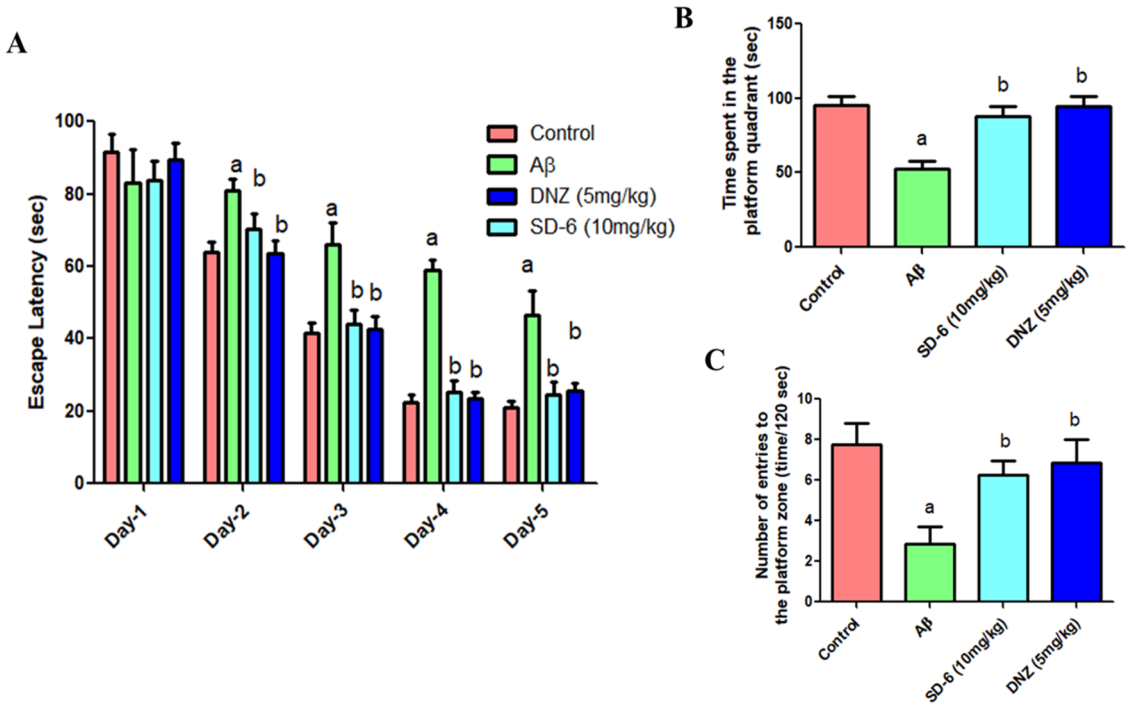

Figure 8. Estimation of **SD-6** and donepezil effects in ICV $A\beta_{1-42}$-induced Morris water maze test: (A) escape latency; (B) time spent in the platform quadrant in the probe trial; and (C) a number of entries to the platform zone during probe trial. All results are expressed in mean ± SEM (n = 6). ($^{a}p < 0.001$ vs control and $^{b}p < 0.001$ vs an Aβ).

was performed post-treatment in the animals of each group, and the time to find the hidden submerged platform, *i.e.*, escape latency (EL) time (ELT), the total number of entries to the platform zone, and time spent in the platform quadrant, was predicted for 90 s as a test of retention of memory. The results of the test exhibited an initial extension in the escape latency time in all groups of animals on day 1, while it declined significantly in other groups as compared to the Aβ group. The donepezil treatment group has shown a maximum decline in ELT over the 5 days as compared to the Aβ group. The treatment group with compound **SD-6** has also demonstrated a nonsignificant change in ELT as compared to the donepezil-treated group, while it has demonstrated a significant change as compared to the Aβ group (Figure 8A). The retention of memory was estimated by the time spent in the platform zone, which was significantly ($^{b}p < 0.001$) higher for the donepezil (5 mg/kg) and **SD-6**-treated group as compared to that for the Aβ-treated group (Figure 8B). The effect on the search accuracy of compound **SD-6** was estimated through the total entries to the platform zone. The animals treated with donepezil and **SD-6** showed nonsignificant ($^{a}p < 0.001$) results in the total number of entries to the platform zone as compared to the control group, while the results were significantly ($^{b}p < 0.001$) different from the Aβ-treated animal group (Figure 8C).

2.4.4. Ex Vivo Biochemical Estimation. The neurochemical effects of compound **SD-6** were studied by *ex vivo* biochemical estimation in scopolamine-treated rat brains (hippocampal). The *ex vivo* AChE estimation was performed using a modified Ellman's method.[47] The results exhibited that the AChE level was significantly ($^{a}p < 0.001$) higher in scopolamine-treated group as compared to that in the control group and showed a dose-dependent decrease in AChE levels in the **SD-6**-treated (2.5, 5, and 10 mg/kg) groups (Figure 9A). The animals treated with **SD-6** (10 mg/kg) showed a statistically nonsignificant difference to that of the donepezil (5 mg/kg)-treated group as compared with the control group, while it has shown significant ($^{b,c,d}p < 0.001$) difference from the scopolamine-treated group.

The acetylcholine (ACh) level in the brain was also analyzed as per the manufacturer's protocol (rat acetylcholine ACh GENLISA ELISA kit, KRISHGEN Biosystems) and suggested a dose-dependent increase in the ACh brain level in the **SD-6**-treated rat group. The results of the 10 mg/kg treatment group of **SD-6** were found to be statistically nonsignificant with the donepezil 5 mg/kg-treated group as compared to that of the control group, while the results were significantly different ($^{b,c,d}p < 0.001$) from the scopolamine-treated group (Figure 9B).

The estimation of biomarkers like malonaldehyde (MDA) and superoxide dismutase (SOD) (oxidative stress biomarkers) in the brain hippocampal homogenates was performed to evaluate the MDA, a byproduct of lipid peroxidation reaction and dismutation of the superoxide radicals into free oxygen as the measure of SOD. Our *ex vivo* findings suggested that scopolamine administration induces oxidative stress and elevates MDA levels; meanwhile, it declines the superoxide dismutation and so the SOD levels. In the **SD-6**-treated group, declines in MDA and elevation of SOD levels were observed in a dose-dependent (2.5, 5, and 10 mg/kg) manner and were found that the results of **SD-6** (10 mg/kg) and donepezil (5 mg/kg) were significantly different ($^{b,c,d}p < 0.001$) than scopolamine-treated groups and were also nonsignificant to the control group (Figure 9C,D). The estimation of GSH (ROS neutralization capabilities) and catalase activity (conversion of H_2O_2 into the water and free oxygen) was also determined in the brain hippocampal homogenate, which resulted in the dose-dependent (2.5, 5, and 10 mg/kg of **SD-6**)

https://doi.org/10.1021/acsomega.2c08061
ACS Omega 2023, 8, 9394−9414

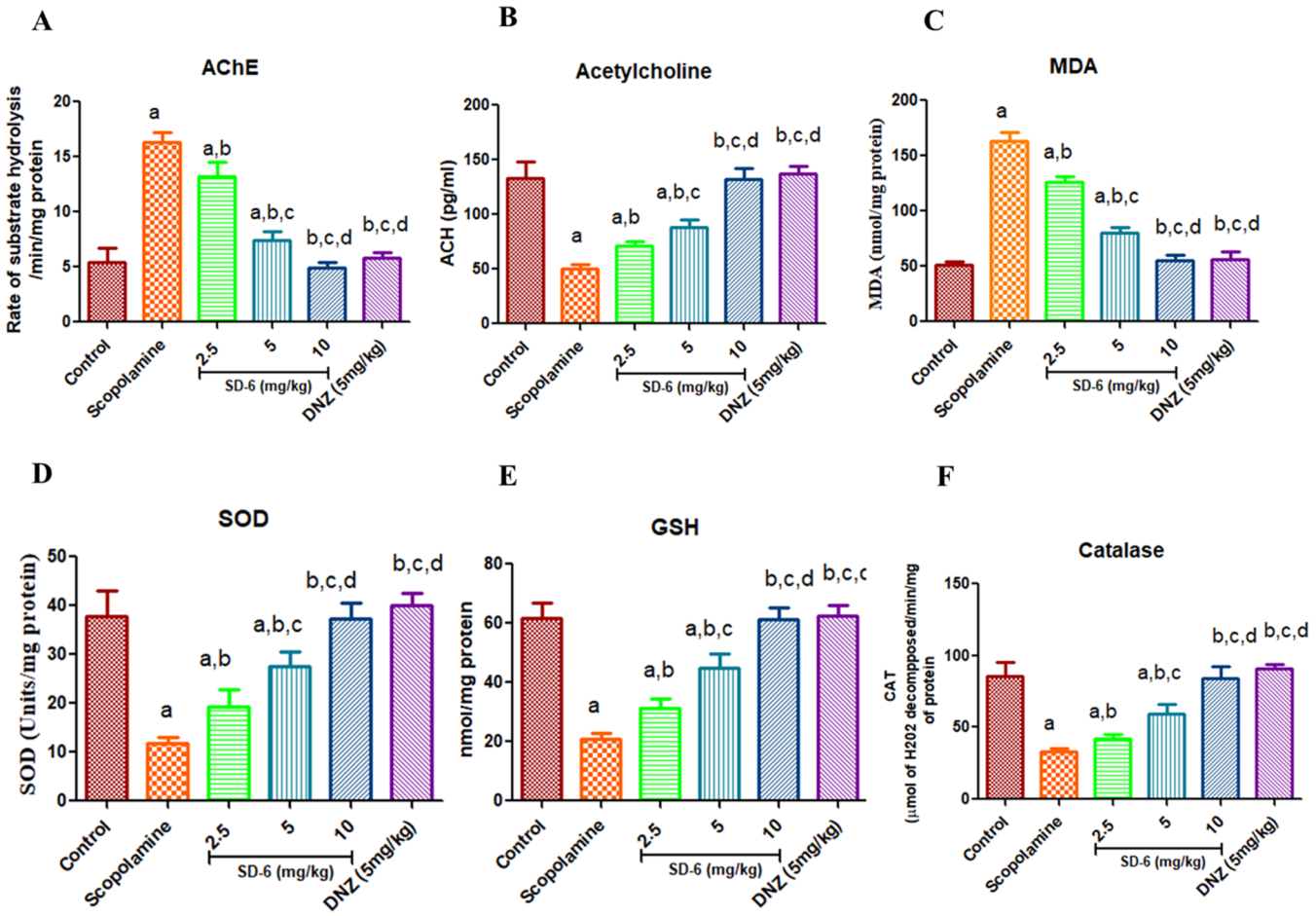

Figure 9. *Ex vivo* studies of compound **SD-6** to estimate the levels of (A) AChE, (B) acetylcholine (ACh), (C) malonaldehyde (MDA), (D) superoxide dismutase (SOD), (E) glutathione (GSH), and (F) catalase. The results are expressed as mean ± SEM ($n = 6$), ($^{a}p < 0.001$) vs control. ($^{a,b}p < 0.05$), (^{a,b,c} $p < 0.01$), and ($^{b,c,d}p < 0.001$) vs scopolamine.

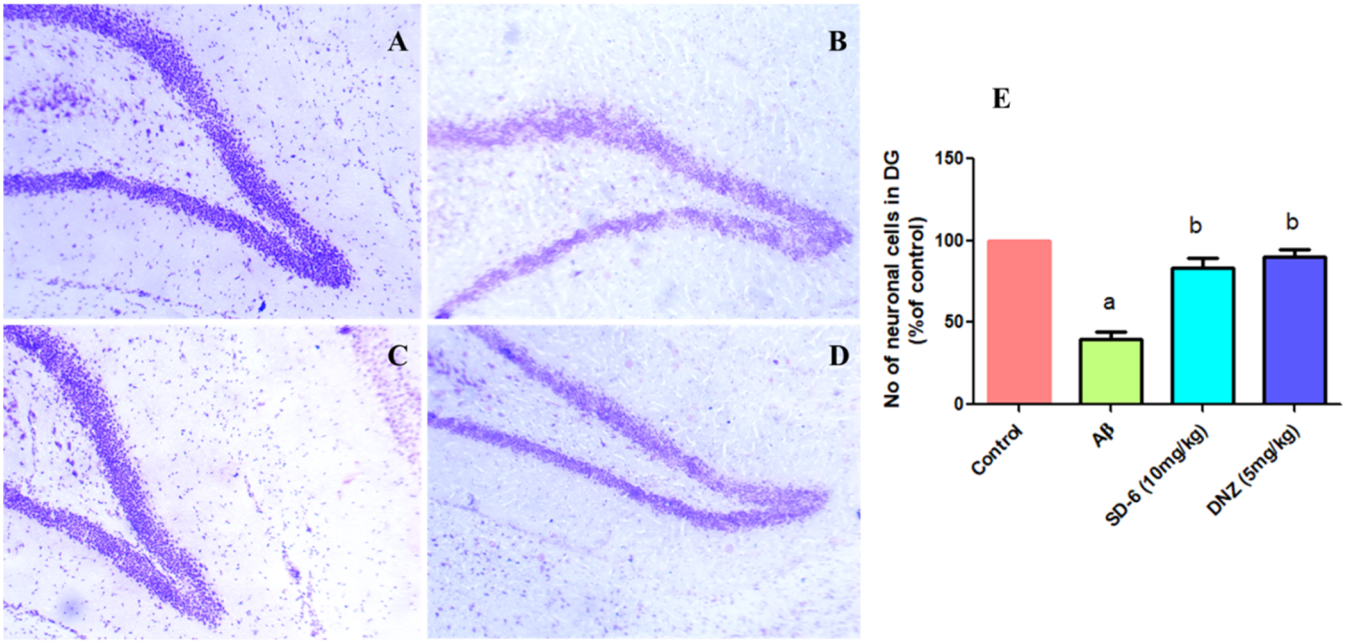

Figure 10. Histomorphological representation dentate gyrus (DG) region of brain hippocampal of the control (A); Aβ_{1-42}-treated group (B); **SD-6**-treated (10 mg/kg) group (C); donepezil (DNZ)-treated (5 mg/kg) group (D); and density graph of the total neuronal cells (% of control) present in DG (E).

https://doi.org/10.1021/acsomega.2c08061
ACS Omega 2023, 8, 9394−9414

elevation of both the biomarkers. The **SD-6**- (10 mg/kg) and donepezil (5 mg/kg)-treated group showed statistically significant ($^{b,c,d}p < 0.001$) differences in GSH and catalase levels as compared with the scopolamine-treated group (Figure 9E,F).

2.4.5. Animal Brain Tissue Histopathology. The rat brain tissue histopathology was performed in control, Aβ_{1-42}, **SD-6**-, and donepezil-treated groups, and neuronal morphology and density were examined after the Nissl staining protocol. The histopathological examination of the group infused with Aβ_{1-42} has resulted in a disordered arrangement of neurons and the formation of vacuolar fibers (Figure 10A,B) along with the decline in neuronal density as compared with the control group. However, the histopathological examination of the hippocampal brain (dentate gyrus (DG)) treated with **SD-6** (10 mg/kg) and donepezil (5 mg/kg) has resulted in less disordered neuronal arrangement and vacuolar fibrosis (Figure 10C,D), while the neuronal density (Figure 10E) was also higher in these groups as compared to that of the Aβ_{1-42}-treated group.

2.5. *In Silico* Studies. *2.5.1. Molecular Dockings.* The rigid molecular docking studies of compounds **SD-4** and **SD-6** were performed using the Glide XP module of the Schrödinger Maestro 2018.1 on Linux-based workstation. In the rigid molecular docking studies, the protein was considered rigid, whereas all degrees of the freedom of the ligands (flexible) were explored to achieve optimum interaction with the protein. Initially, the docking protocols were validated by extracting and redocking the cocrystallized bound ligand (donepezil for hAChE and F1M for hBACE-1) in the active site of both the enzymes and calculated the root-mean-square deviation (RMSD) value, which was found to be 1.50 and 1.20 Å (acceptable range ≤2 Å) for hAChE and hBACE-1, respectively. The superimposition and XP visualizer tools were used to study the binding modes of the cocrystallized and redocked ligands to ascertain the validation of the prepared grid and docking protocols. The docking studies affirmed the consensual binding pattern of both the compounds in the active site of the enzymes hAChE (PDB: 4EY7) and hBACE-1 (PDB: 2ZJM).

The docking result of compounds **SD-4** and **SD-6** against hAChE suggested that the phenyl and 1,3,4-oxadiazole-2-thione rings of the compounds were interacting with the Trp286 and Tyr341 residues of the AChE-PAS region *via* strong hydrophobic $\pi-\pi$ stacking interaction, while compound **SD-6** showed an additional $\pi-\pi$ stacking interaction with the Tyr124 residue of the AChE-PAS region. One of the protonated nitrogen atoms of the BP ring present in both compounds was interacting with the Trp86 residue of the anionic subsite by $\pi-$cationic interactions. The benzyl ring of both the compounds was also interacting with the acyl-binding pocket residues Gly120, Gly121, and Gly122 *via* glycine-rich interactions and AChE-CAS residues His447 and Ser203 *via* polar interactions (Figures S4A,B and S5A,B). However, the benzyl ring of **SD-6** was interacting with His447 *via* an additional $\pi-\pi$ stacking interaction (Figure S5A,B) corroborating its *in vitro* hAChE inhibitory activity. The docked pose superimposition of compounds **SD-4**, **SD-6**, and donepezil in the hAChE active site suggested that all three compounds are almost aligned in the same plan and share common amino acid residue interactions (Figure S4E).

The molecular docking results of compounds **SD-4** and **SD-6** against hBACE-1 suggested that the protonated nitrogen of the BP ring present in both the compounds was interacting with the catalytic dyad residues Asp32 and Asp228 *via* salt bridge interaction, which is necessary for inhibition of the enzymatic activity. However, the phenyl ring of both the compounds was interacting with the Tyr71 residue *via* $\pi-\pi$ stacking interaction. The 3-C≡N group present in the phenyl ring of **SD-4** also exhibited water-mediated H-bond interaction with the Ser36; the benzyl ring showed $\pi-\pi$ stacking interaction with the Trp115 residue, while an oxygen atom of 1,3,4-oxadiazole-2-thione of **SD-6** showed H-bond interaction with the Tyr198 residue (Figures S4C,D and S5C,D). The presence of H-bond and $\pi-\pi$ stacking interaction other than catalytic dyad residue interactions is believed to be accountable for better BACE-1 inhibitory potential of compounds **SD-4** and **SD-6**. The docked pose superimposition of compounds **SD-4**, **SD-6**, and F1M in the active site of the BACE-1 suggested that all compounds were interacting with the catalytic dyad residues (Asp32 and Asp228) and sharing almost the same plane (Figure S4F). The overall molecular docking studies of compounds **SD-4** and **SD-6** against hAChE and hBACE-1 enzymes confirmed their binding with the hAChE-CAS, PAS residues, and the catalytic dyad residues of the hBACE-1 enzymes, respectively, which are in complete agreement of the *in vitro* (**SD-4** and **SD-6**) and *in vivo* (**SD-6**) studies of the compounds.

The molecular docking studies of compounds **SD-4** and **SD-6** were also performed against the hBChE enzyme (PDB: 4TPK) to see the interaction of both the compounds in the active site of the enzyme (Figures S5E,F and S6A–D), suggesting that both the molecules are interacting with the CAS and PAS residues of the enzymes and sharing the same plan to that of the rivastigmine (BChE inhibitor) in the hBChE active site. The glide scores (kcal/mol) of compounds **SD-4** and **SD-6** against hAChE, hBChE, and hBACE-1 were also determined using the Glide XP visualizer module of the Schrödinger 2018-1, and the results suggested that the Glide scores of both the compounds were comparable to standard molecules donepezil, rivastigmine, and F1M for hAChE, hBChE, and hBACE-1, respectively (Table 4).

2.5.2. Molecular Dynamics (MD). To understand the stability of the docked complex, a molecular dynamic (MD) simulation run of 100 ns was performed for both the ligand–protein complex (**SD-4** and **SD-6** with hAChE, hBChE, and BACE-1). The Desmond module of the Schrödinger suite was utilized to run the MD studies of the complexes on the graphical processing unit (GPU). The MD results of both the docked complex have shown that the root-mean-square deviation (RMSD) value was within the acceptable range of 1–3 Å with stable trajectories during the entire run of 100 ns. The protein–ligand root-mean-square fluctuations (RMSFs) were also found within the range under 3 Å. The "simulation interaction diagram" tool of Desmond was used to understand the protein–ligand interaction through PL-histogram, PL-RMSD, PL-timeline, and PL-2D interaction diagrams.

The MD simulation results of compounds **SD-4** and **SD-6** against hAChE suggested that the phenyl ring of both the compounds was interacting with the Trp86 (100%) and Trp286 (70%), respectively, *via* the face-to-face $\pi-\pi$ stacking interaction. The protonated nitrogen atom of the BP ring of **SD-4** and **SD-6** interacted with the anionic subsite residue Glu202 (87%) and AChE-PAS residue Asp74 (99%), respectively, *via* H-bond interaction. Compound **SD-4** demonstrated a strong hydrophobic $\pi-\pi$ stacking interaction

https://doi.org/10.1021/acsomega.2c08061
ACS Omega 2023, 8, 9394–9414

Table 3. Absorption, Distribution, Metabolism, and Excretion (ADME)-Predicted Properties of the Compounds and Standard Drugs[a]

compound code	SASA	donor HB	accept HB	QPlog Po/w	QPPCaco	Qplog BB	%HOA	rule of five	QppMDCK
SD-4	722.8	0	9	2.18	82.84	0.22	74.07	0	94.90
SD-6	684.9	0	7.5	3.02	398.88	1.075	89.95	0	534.34
donepezil	720.2	0	5.5	4.47	893.17	0.11	100	0	484.39
rivastigmine	565.2	0	5	2.48	1086.04	0.38	95.83	0	617.56

[a]SASA total solvent-accessible surface area in square angstroms (range 300−1000 Å), donor HB H-bond donors (range 0−6), accept H-bond acceptor (range 2−20), QPlog Po/w predicted log of octanol/water partition coefficient (range 2−6), QPPCaco predicted apparent Caco-2 cell permeability in nm/s (range <25 poor, >500 great), QPlog BB predicted brain/blood partition coefficients (range −3 to 1.2), %HOA predicted human oral absorption (>80% is high, <25% is poor), QppMDCK cells are considered to be a good mimic for the BBB (<25—poor; >500—great).

with the AChE-CAS residue His447 (74%), while the sulfur atom of the 1,3,4-oxadiazole-2-thione ring of **SD-6** showed water bridge interaction with Phe295 (64%) and Arg296 (49%) of acyl-binding pocket. Compound **SD-6** showed an additional hydrophobic $\pi-\pi$ stacking interaction with AChE-PAS residue Tyr72 (50%) and Tyr341(95%), imparting its strong hAChE inhibition potential (Figures S7 and S10).

The MD simulation studies of compound **SD-4** and **SD-6** complexed with hBACE-1 also suggested that the protonated nitrogen atom of the BP ring was interacting with the catalytic dyad residues Asp32 (100 and 87%) *via* H-bond interaction and Asp228 (90 and 100%) *via* ionic bond interaction. The phenyl ring of compounds **SD-4** and **SD-6** showed $\pi-\pi$ stacking interaction with Tyr71 (38 and 58%), while the BP ring of compound **SD-4** showed an additional $\pi-\pi$ stacking interaction with Tyr71 (36%). The 3-C≡N group present on the phenyl ring of the **SD-4** showed H-bond interaction with the Asn37 (37%), while the sulfur atom of the 1,3,4-oxadiazole-2-thione ring of **SD-6** showed water bridge interaction with the Arg235 (33%) residue (Figures S9 and S12), suggesting a more stable confirmation of **SD-6** over **SD-4** with BACE-1.

The MD simulation studies of compounds **SD-4** and **SD-6** complexed with hBChE have also been performed to see the stability of both the docked complexes. The results of the MD studies suggested that the protonated nitrogen atom of the BP ring present in both compounds was interacting with the BChE-PAS residue Asp70 (100%) *via* strong H-bond interaction. Compound **SD-4** showed hydrophobic $\pi-\pi$ stacking interaction with the anionic subsite residue Trp82 (90%), while compound **SD-6** showed strong hydrophobic $\pi-\pi$ stacking interactions with the anionic subsite residue Trp82 (100%) and the acyl-binding pocket residues Trp231 (80%) and Phe329 (100%) (Figures S8 and S11).

The molecular dockings and dynamics results of both compounds **SD-4** and **SD-6** also corroborate our *in vitro* and *in vivo* findings that both of these compounds are representative molecules of the series and **SD-6** was the most suitable compound for the *in vivo* experiments.

2.5.3. In Silico Determination of Drug-Like Properties. To target any molecule in the central nervous system (CNS), the estimation of its physicochemical parameters is crucial in developing a drug-like molecule. The various parameters of molecules **SD-4** and **SD-6** were predicted using the Quikprop module of the Schrodinger such as the total solvent-accessible surface area (SASA), donor HB, accept HB, octanol/water partition coefficient (QPlog Po/w), Caco-2 cell permeability (QPPCaco), brain/blood partition coefficient (QPlog BB), % human oral absorption (%HOA), Lipinski's rule of five, and predicted apparent MDCK cell permeability (QPPMDCK). The predicted properties of both the molecules were compared with the standard drugs donepezil and rivastigmine, which suggested that compounds **SD-4** and **SD-6** retain drug-like properties in the acceptable limits with high BBB permeation capability (Table 3). The drug-likeness properties of compound **SD-6** have also revealed that it was the most promising molecule of the series and so did the *in vitro* and *in vivo* activities.

2.5.4. Binding Free Energy (MM/GBSA) Calculation. The molecular mechanics/generalized Born surface area (MM/GBSA) was used to predict the binding free energy (ΔG_{bind} in kcal/mol) between the protein and ligand. The binding free energy was calculated based on the combination of gas-phase energy (MM), electrostatic solvation energy (GB), and nonelectrostatic contribution to solvation energy (SA). The ΔG_{bind} energy of both compounds **SD-4** and **SD-6** was calculated and compared with the standard donepezil, rivastigmine, and F1M molecules using the prime MM/GBSA module of Schrödinger 2018-1. The detailed results are expressed in Table 4 and suggested that the ΔG_{bind} energy of compounds **SD-4** and **SD-6** was comparable to donepezil, rivastigmine, and F1M molecules against hAChE and hBACE-1 enzymes, while ΔG_{bind} energy of both the compounds was better than the standard donepezil, rivastigmine, and F1M against the hBChE enzyme.

Table 4. Results of Docking (Glide Score) and MM/GBSA

enzyme	compound	glide score[a]	ΔG binding energy[a]
hAChE	donepezil	−14.150	−65.258
	rivastigmine	−13.150	−55.196
	F1M	−15.005	−58.482
	SD-4	−15.120	−61.425
	SD-6	−13.746	−62.166
hBChE	rivastigmine	−4.969	−35.037
	donepezil	−7.212	−48.086
	F1M	−6.590	−36.773
	SD-4	−6.961	−54.993
	SD-6	−7.759	−63.777
hBACE-1	F1M	−7.641	−63.257
	donepezil	−5.782	−58.023
	rivastigmine	−5.158	−39.593
	SD-4	−6.312	−51.650
	SD-6	−6.191	−51.709

[a]Glide scores and ΔG binding energy are calculated in kcal/mol.

3. CONCLUSIONS

Compounds **SD-4** and **SD-6** have shown multitargeting inhibitory effects in a micromolar to nanomolar range. Both

https://doi.org/10.1021/acsomega.2c08061
ACS Omega 2023, 8, 9394−9414

compounds have shown ChE-inhibitory potential comparable to standard donepezil and rivastigmine, while BACE-1 inhibition of both compounds was better than donepezil. Along with good enzymatic inhibitory potential, both compounds have displayed anti-Aβ aggregation, PI displacement, and BBB permeability better than donepezil at their tested concentrations.

The *in vivo* behavioral Y-maze test (scopolamine-induced) and Aβ-induced (AD-phenotypic model) Morris water maze test results suggested that compound **SD-6** has the capability to ameliorate both cholinergic and Aβ-induced memory and cognitive deficits. The *ex vivo* study of the brain hippocampal region suggested an increase in ACh, SOD, GSH, and catalase levels, while a decline in AChE and MDA levels in a dose-dependent manner. However, the histopathological examination of brain slices demonstrated an improvement in neuronal density and DG morphology in **SD-6**-treated animals. The *in silico* dockings and MD simulation studies also corroborate our *in vitro* and *in vivo* findings. The Quikprop analysis suggested drug-like properties, while MM/GBSA results suggested minimum ΔG_{bind} energy of ligand−protein complexes. Finally, it can be concluded based on our experimental findings that compound **SD-6** is a lead candidate to be explored more in AD therapy.

4. EXPERIMENTAL SECTION

4.1. Chemistry. *4.1.1. Chemicals and Instrumentation.* The reagents and chemicals utilized in the experimental work were procured from TCI Chemicals, Sigma-Aldrich, and Avra Synthesis, India, and utilized without further purification otherwise stated by the manufacturer. The progress and compellation of the reaction were observed, and the R_f value of the compounds was also calculated by Merck silica gel 60F254 precoated aluminum plates (Merck Germany). The visualization of the thin-layer chromatography (TLC) plates was performed under a UV light-enabled closed TLC cabinet using iodine vapors, Dragendorff's reagent, or Ninhydrin reagent. The melting points of the compounds were determined using the Stuart melting point apparatus (SPM10) in capillary tubes and are reported as uncorrected melting points. The FT-IR spectra of the compounds were recorded as % transmittance vs wavenumber (cm^{-1}) on an α ECO-ATR spectrophotometer (Bruker). ^{1}H NMR (500 MHz) and ^{13}C NMR (126 MHz) spectra of the synthesized compounds were captured on a Bruker Avance 500 MHz spectrophotometer using tetramethylsilane (TMS) as a reference standard in dimethyl sulfoxide (DMSO)-d_6 or $CDCl_3$. The % purity of the compounds was determined through high-performance liquid chromatography (Shimadzu) using 1 mL/min flowrate of ACN/H_2O/trifluoroacetic acid (TFA) (95:5:0.1%) as the mobile phase in the C_{18} column. The HRMS spectra of the compounds were recorded on an AB Sciex X500R QTOF mass spectrometer.

*4.1.2. General Procedure for the Synthesis of Compounds (**B1−17**).* Compounds **B1−17** were synthesized as per the procedure reported previously from our lab.[26] To a suspension of different substituted benzoic acids (1 equiv) in acetonitrile, HOBT (1.2 equiv), and EDC·HCl (1.2 equiv) was added at room temperature and the reaction was monitored for the total conversion of acid to ester through TLC using hexane/EtOAc (50:50 v/v). After the full conversion of acid to ester, this suspension was added dropwise to a mixture of hydrazine hydrate (2 equiv) in acetonitrile previously kept at 0−5 °C. The reaction was further allowed to be stirred at room temperature and monitored by TLC using hexane/EtOAc (50:50 v/v). After completion, the reaction mixture was quenched with water and extracted with EtOAc (3 × 50 mL) and washed with saturated $NaHCO_3$ and brine solution, dried over Na_2SO_4, and the solvent was evaporated to dryness to get pure compounds **B1−17**, which was used in the next step without further purification.

*4.1.3. General Procedure for the Synthesis of Compounds (**C1−17**).* Compounds **C1−17** were synthesized as per the procedure reported,[48] and the appropriate amount of substituted aryl hydrazides (1 equiv) in ethanol was taken into two necks of round-bottom flask under an inert atmosphere. Potassium hydroxide (1 equiv) was added to the ethanolic solution, and an excess amount of carbon disulfide (2.5 equiv) was added dropwise to it. The reaction mixture was stirred and refluxed for 4−6 h and monitored by TLC using hexane/EtOAc (50:50 v/v). After completion of the reaction, the solvent was evaporated under reduced pressure, followed by the addition of water, and 3 M HCl was used to adjust the pH 2−3 to get a complete precipitate. The precipitate was further washed with water to remove HCl and recrystallized with ethanol to obtain products **C1−17** in pure form.[48]

*4.1.4. General Procedure for the Synthesis of Compounds (**SD-1−17**).* To a hot solution of **C1−17** (0.005 mol) in ethanol benzylpiperazine (0.01 mol) and 37% formaldehyde solution (1.0 mL) was added and the mixture was stirred at room temperature for 5 h. The reaction mixture was allowed to stand overnight, and 5 mL of water was added dropwise for 1 h with continuous stirring. The precipitate formed was filtered and washed with water thrice, dried, and recrystallized further with ethanol to get the desired product **SD-1−17**.[49]

*4.1.4.1. 3-((4-Benzylpiperazin-1-yl)methyl)-5-(4-chlorophenyl)-1,3,4-oxadiazole-2(3H)-thione (**SD-1**).* Yellow solid, yield 72%, mp 226−228 °C; TLC (EtOAc/hexane, 80:20 v/v); R_f = 0.54. FT-IR (α ATR, ν cm^{-1}): 3045 (Ar−CH), 2954 (CH methylene) 1280 (C═S), 1656 (C−N); ^{1}H NMR (500 MHz, $CDCl_3$) δ 7.97−7.93 (m, 2H), 7.60−7.50 (m, 3H), 7.26 (dd, J = 8.2, 5.6 Hz, 2H), 6.99 (dd, J = 12.1, 5.1 Hz, 2H), 5.11 (s, 2H), 3.47 (s, 2H), 2.91 (t, J = 4.6 Hz, 4H), 2.48 (s, 4H). ^{13}C NMR (126 MHz, $CDCl_3$) δ 178.28, 162.99, 161.05, 158.93, 133.68, 133.66, 132.38, 130.61, 130.55, 129.16, 126.52, 122.44, 115.10, 114.93, 70.33, 62.15, 52.83, 50.21; HRMS $[M + 1]^+$ calcd 400.1125, found 400.1139; HPLC purity: 96.55%; retention time: 3.8 min.

*4.1.4.2. 3-((4-Benzylpiperazin-1-yl)methyl)-5-(4-nitrophenyl)-1,3,4-oxadiazole-2(3H)-thione (**SD-2**).* White solid, yield 75%, mp 219−221 °C; TLC (EtOAc/hexane, 80:20 v/v); R_f = 0.60. FT-IR (α ATR, ν cm^{-1}): 3134 (Ar−CH), 2937 (CH methylene) 1218 (C═S), 1658 (C−N); ^{1}H NMR (500 MHz, DMSO-d_6) δ 8.56 (d, J = 7.06 Hz, 2H), 7.94−7.92 (t, J = 6.01 Hz, 2H), 7.91−7.61 (m, 5H), 5.11 (s, 2H), 5.09 (s, 2H), 3.12 (s, 4H), 2.99 (s, 4H). ^{13}C NMR (126 MHz, DMSO-d_6) δ 159.07, 138.37, 133.12, 131.74, 130.05, 129.63, 126.72, 126.68, 90.99, 71.96, 69.84, 45.46, 43.39; HRMS $[M + 1]^+$ calcd 411.1365, found 411.1352; HPLC purity: 97.32%; retention time: 3.6 min.

*4.1.4.3. 3-((4-Benzylpiperazin-1-yl)methyl)-5-(4-(trifluoromethoxy)phenyl)-1,3,4-oxadiazole-2(3H)-thione (**SD-3**).* Light yellow solid, yield 71%, mp 224−226 °C; TLC (EtOAc/hexane, 80:20 v/v); R_f = 0.61. FT-IR (α ATR, ν cm^{-1}): 3066 (Ar−CH), 2941 (CH methylene) 1264 (C═S), 1639 (C−N); ^{1}H NMR (500 MHz, $CDCl_3$) δ 7.99 (d, J = 7.9

https://doi.org/10.1021/acsomega.2c08061
ACS Omega 2023, 8, 9394−9414

Hz, 2H), 7.60−7.53 (m, 2H), 7.40 (d, J = 7.5 Hz, 3H), 7.18 (dd, J = 7.9, 6.4 Hz, 2H), 5.11 (d, J = 1.7 Hz, 2H), 4.24 (s, 2H), 2.92 (s, 4H), 2.46 (s, 4H). ^{13}C NMR (126 MHz, $CDCl_3$) δ 178.38, 158.97, 142.57, 132.38, 129.19, 128.50, 127.89, 126.97, 126.58, 122.55, 76.15, 70.35, 51.77, 50.50; HRMS $[M + 1]^+$ calcd 450.1337, found 450.1316; HPLC purity: 96.77%; retention time: 3.2 min.

*4.1.4.4. 3-(4-((4-Benzylpiperazin-1-yl)methyl)-5-thioxo-4,5-dihydro-1,3,4-oxadiazol-2-yl)benzonitrile (**SD-4**).* White solid, yield 76%, mp 220−222 °C; TLC (EtOAc/hexane, 80:20 v/v); R_f = 0.58. FT-IR (α ATR, ν cm^{-1}): 3086 (Ar−CH), 2814 (CH methylene) 1288 (C═S), 1651 (C−N); ^{1}H NMR (500 MHz, DMSO-d_6) δ 8.28 (s, 1H), 8.18 (d, J = 7.9 Hz, 1H), 8.07 (d, J = 7.0 Hz, 1H), 7.83−7.75 (m, 1H), 7.42−7.20 (m, 5H), 5.06 (s, 2H), 3.51 (s, 2H), 2.80 (s, 4H), 2.44 (s, 4H). ^{13}C NMR (126 MHz, DMSO-d_6) δ 131.18, 129.44, 128.65, 127.58, 118.23, 114.00, 113.07, 70.44, 62.20, 52.74, 49.71; HRMS $[M + 1]^+$ calcd 391.1467, found 391.2856; HPLC purity: 98.22%; retention time: 3.9 min.

*4.1.4.5. 3-((4-Benzylpiperazin-1-yl)methyl)-5-(2-nitrophenyl)-1,3,4-oxadiazole-2(3H)-thione (**SD-5**).* Light yellow solid, yield 72%, mp 221−223 °C; TLC (EtOAc/hexane, 80:20 v/v); R_f = 0.55. FT-IR (α ATR, ν cm^{-1}): 3078 (Ar−CH), 2954 (CH methylene) 1252 (C═S), 1643 (C−N); ^{1}H NMR (500 MHz, $CDCl_3$) δ 7.99−7.89 (m, 2H), 7.62−7.49 (m, 3H), 6.95−6.82 (m, 4H), 5.16 (s, 2H), 3.76 (d, J = 1.6 Hz, 2H), 3.10 (d, J = 4.3 Hz, 4H), 3.07−3.02 (m, 4H). ^{13}C NMR (126 MHz, $CDCl_3$) δ 178.32, 159.06, 154.11, 145.63, 132.43, 129.19, 126.56, 122.42, 118.65, 114.48, 70.30, 55.57, 50.87, 50.40; HRMS $[M + 1]^+$ calcd 411.1365, found 411.1338; HPLC purity: 96.85%; retention time: 4.1 min.

*4.1.4.6. 3-((4-Benzylpiperazin-1-yl)methyl)-5-phenyl-1,3,4-oxadiazole-2(3H)-thione (**SD-6**).* White solid, yield 78%, mp 218−220 °C; TLC (EtOAc/hexane, 80:20 v/v); R_f = 0.60. FT-IR (α ATR, ν cm^{-1}): 3051 (Ar−CH), 2811 (CH methylene) 1231 (C═S), 1651 (C−N); ^{1}H NMR (500 MHz, $CDCl_3$) δ 7.95 (d, J = 7.4 Hz, 2H), 7.55 (ddd, J = 10.5 Hz, 3H), 7.33−7.23 (m, 5H), 5.11 (s, 2H), 3.52 (s, 2H), 2.92 (s, 4H), 2.51 (s, 4H). ^{13}C NMR (126 MHz, $CDCl_3$) δ 178.27, 158.94, 137.81, 132.38, 129.21, 129.17, 128.25, 127.14, 126.53, 122.43, 70.33, 63.00, 52.90, 50.19; HRMS $[M + 1]^+$ calcd 366.1514, found 366.3757; HPLC purity: 99.04%; retention time: 3.5 min.

*4.1.4.7. 3-((4-Benzylpiperazin-1-yl)methyl)-5-(3-chlorophenyl)-1,3,4-oxadiazole-2(3H)-thione (**SD-7**).* Orange solid, yield 69%, mp 226−228 °C; TLC (EtOAc/hexane, 80:20 v/v); R_f = 0.51. FT-IR (α ATR, ν cm^{-1}): 3118 (Ar−CH), 2837 (CH methylene) 1268 (C═S), 1680 (C−N); ^{1}H NMR (500 MHz, DMSO-d_6) δ 8.26 (s, 1H), 7.88 (dt, J = 7.43, 2.6 Hz, 1H), 7.48 (dt, J = 7.4, 3.2 Hz, 1H), 7.42 (t, J = 7.4 Hz, 1H), 7.32−7.27 (m, 5H), 5.16 (s, 2H), 3.41 (s, 2H), 2.68 (s, 4H), 2.59 (s, 4H). ^{13}C NMR (126 MHz, DMSO-d_6) δ 164.92, 161.36, 134.80, 133.86, 132.52, 132.33, 130.16, 129.41, 127.73, 126.68, 64.84, 61. 89, 50.91, 48.14; HRMS $[M + 1]^+$ calcd 400.1125, found 400.1102; HPLC purity: 96.33%; retention time: 3.6 min.

*4.1.4.8. 3-((4-Benzylpiperazin-1-yl)methyl)-5-(4-(trifluoromethyl)phenyl)-1,3,4-oxadiazole-2(3H)-thione (**SD-8**).* Light yellow solid, yield 70%, mp 225−227 °C; TLC (EtOAc/hexane, 80:20 v/v); R_f = 0.54. FT-IR (α ATR, ν cm^{-1}): 3066 (Ar−CH), 2847 (CH methylene) 1259 (C═S), 1668 (C−N); ^{1}H NMR (500 MHz, DMSO) δ 7.91 (s, 2H), 7.55−7.53 (m, 5H), 7.48 (s, 2H), 5.57 (s, 2H), 5.19 (s, 2H), 2.80 (s, 4H), 2.39 (s, 4H). ^{13}C NMR (126 MHz, DMSO) δ 168.57, 152.24, 148.65, 131.34, 131.07, 129.25, 128.80, 127.36, 125.63, 116.20, 69.47, 62.48, 52.96, 50.35; HRMS $[M + 1]^+$ calcd 434.1388, found 434.1361; HPLC purity: 95.89%; retention time: 4.2 min.

*4.1.4.9. 3-((4-Benzylpiperazin-1-yl)methyl)-5-(2,4-dichlorophenyl)-1,3,4-oxadiazole-2(3H)-thione (**SD-9**).* White solid, yield 72%, mp 227−229 °C; TLC (EtOAc/hexane, 80:20 v/v); R_f = 0.61. FT-IR (α ATR, ν cm^{-1}): 3109 (Ar−CH), 2856 (CH methylene) 1242 (C═S), 1649 (C−N); ^{1}H NMR (500 MHz, $CDCl_3$) δ 7.95 (dt, J = 3.9, 2.5 Hz, 2H), 7.85-7.49 (m, 3H), 7.21−7.10 (m, 3H), 5.11 (s, 2H), 3.47 (d, J = 5.1, 2H), 2.91 (s, 4H), 2.48 (s, Hz, 4H). ^{13}C NMR (126 MHz, $CDCl_3$) δ 176.65, 159.77, 154.10, 140.43, 140.05, 132.73, 132.53, 132.34, 129.25, 129.21, 126.52, 126.45, 122.12, 65.52, 61.01, 60.97, 58.66, 56.83; HRMS $[M + 1]^+$ calcd 434.0735, found 434.0752; HPLC purity: 96.86%; retention time: 3.7 min.

*4.1.4.10. 3-((4-Benzylpiperazin-1-yl)methyl)-5-(4-hydroxyphenyl)-1,3,4-oxadiazole-2(3H)-thione (**SD-10**).* Light yellow solid, yield 58%, mp 214−216 °C; TLC (EtOAc/hexane, 80:20 v/v); R_f = 0.42. FT-IR (α ATR, ν cm^{-1}): 3098 (Ar−CH), 2953 (CH methylene) 1268 (C═S), 1644 (C−N); ^{1}H NMR (500 MHz, $CDCl_3$) δ 10.22 (s, 1H), 8.04−7.86 (m, 2H), 7.60−7.49 (m, 3H), 7.38−7.22 (m, 4H), 5.30 (s, 2H), 3.53 (s, 2H), 2.97 (s, 4H), 2.52 (s, 4H). ^{13}C NMR (126 MHz, $CDCl_3$) δ 163.71, 161.83, 148.24, 137.96, 130.98, 130.83, 130.56, 129.24, 128.83, 128.62, 128.22, 127.09, 121.14, 69.54, 63.12, 53.07, 50.51; HRMS $[M + 1]^+$ calcd 382.1463, found 382.1454; HPLC purity: 97.55%; retention time: 4.0 min.

*4.1.4.11. 5-(4-Aminophenyl)-3-((4-benzylpiperazin-1-yl)methyl)-1,3,4-oxadiazole-2(3H)-thione (**SD-11**).* White solid, yield 60%, mp 220−222 °C; TLC (EtOAc/hexane, 80:20 v/v); R_f = 0.44. FT-IR (α ATR, ν cm^{-1}): 3129 (Ar−CH), 2864 (CH methylene) 1232 (C═S), 1661 (C−N); ^{1}H NMR (500 MHz, $CDCl_3$) δ 7.92−7.82 (m, 2H), 7.45 (dd, J = 9.2, 3.1 Hz, 3H), 7.29 (m, J = 7.0 Hz, 3H), 5.74 (s, 2H), 5.25 (s, 2H), 3.54 (s, 3H), 2.98 (s, 4H), 2.58 (s, 4H). ^{13}C NMR (126 MHz, $CDCl_3$) δ 164.57, 164.49, 156.73, 156.63, 148.72, 148.10, 129.68, 128.77, 128.73, 128.65, 128.59, 128.37, 127.48, 121.87, 121.80, 72.79, 69.24, 52.78, 50.00; HRMS $[M + 1]^+$ calcd 381.1623, found 381.1604; HPLC purity: 95.46%; retention time: 3.6 min.

*4.1.4.12. 3-((4-Benzylpiperazin-1-yl)methyl)-5-(3-methoxyphenyl)-1,3,4-oxadiazole-2(3H)-thione (**SD-12**).* Light orange solid, yield 76%, mp 228−230 °C; TLC (EtOAc/hexane, 80:20 v/v); R_f = 0.62. FT-IR (α ATR, ν cm^{-1}): 3018 (Ar−CH), 2926 (CH methylene) 1244 (C═S), 1660 (C−N); ^{1}H NMR (500 MHz, $CDCl_3$) δ 7.97−7.91 (m, 2H), 7.61−7.47 (m, 3H), 7.15 (dd, J = 7.9, 2.8 Hz, 4H), 5.11 (s, 2H), 3.48 (s, 2H), 2.91 (s, 4H), 2.50 (s, 4H), 2.34 (s, 3H). ^{13}C NMR (126 MHz, $CDCl_3$) δ 178.27, 158.91, 136.70, 134.77, 132.35, 129.16, 129.15, 128.91, 126.52, 122.46, 77.31, 77.05, 76.80, 70.35, 62.74, 52.87, 50.23, 21.08; HRMS $[M + 1]^+$ calcd 396.1620, found 396.1609; HPLC purity: 96.14%; retention time: 3.2 min.

*4.1.4.13. 3-((4-Benzylpiperazin-1-yl)methyl)-5-(4-methoxyphenyl)-1,3,4-oxadiazole-2(3H)-thione (**SD-13**).* White solid, yield 71%, mp 227−229 °C; TLC (EtOAc/hexane, 80:20 v/v); R_f = 0.62. FT-IR (α ATR, ν cm^{-1}): 3034 (Ar−CH), 2966 (CH methylene) 1288 (C═S), 1669 (C−N); ^{1}H NMR (500 MHz, DMSO-d_6) δ 7.84 (dd, J = 8.8, 5.4 Hz, 2H), 7.30−7.22 (m, 5H), 7.24−7.14 (dd, J = 8.8, 6.1 Hz, 2H), 5.02 (s, 1H), 3.86 (d, J = 3.5 Hz, 3H), 3.47 (s, 2H), 2.78 (s, 4H), 2.40 (s, 4H). ^{13}C NMR (126 MHz, DMSO-d_6) δ 138.31,

https://doi.org/10.1021/acsomega.2c08061
ACS Omega 2023, 8, 9394−9414

131.98, 129.30, 129.12, 128.62, 127.44, 115.40, 70.21, 62.33, 61.80, 56.06, 52.81, 49.95; HRMS $[M + 1]^+$ calcd 396.1620, found 396.1631; HPLC purity: 96.67%; retention time: 3.8 min.

*4.1.4.14. 3-((4-Benzylpiperazin-1-yl)methyl)-5-(4-chloro-3-nitrophenyl)-1,3,4-oxadiazole-2(3H)-thione (**SD-14**).* White solid, yield 68%, mp 230−232 °C; TLC (EtOAc/hexane, 80:20 v/v); R_f = 0.64. FT-IR (α ATR, ν cm^{-1}): 3121 (Ar−CH), 2956 (CH methylene) 1238 (C═S), 1672 (C═N); ^{1}H NMR (500 MHz, $CDCl_3$) δ 8.16 (d, J = 36.7 Hz, 2H), 7.83 (s, 1H), 7.66 (s, 1H), 7.31 (d, J = 4.3 Hz, 4H), 5.11 (s, 2H), 3.63 (s, 2H), 2.96 (s, 4H), 2.61 (s, 4H). ^{13}C NMR (126 MHz, $CDCl_3$) δ 136.62, 135.23, 130.24, 129.83, 129.44, 129.13, 128.55, 128.40, 127.54, 70.47, 62.71, 52.64, 49.82; HRMS $[M + 1]^+$ calcd 445.0675, found 445.0986; HPLC purity: 97.12%; retention time: 4.1 min.

*4.1.4.15. 3-((4-Benzylpiperazin-1-yl)methyl)-5-(2,4-dinitrophenyl)-1,3,4-oxadiazole-2(3H)-thione (**SD-15**).* Creamy white solid, yield 75%, mp 227−229 °C; TLC (EtOAc/hexane, 80:20 v/v); R_f = 0.60. FT-IR (α ATR, ν cm^{-1}): 3094 (Ar−CH), 2967 (CH methylene) 1281 (C═S), 1682 (C═N); ^{1}H NMR (500 MHz, $CDCl_3$) δ 8.96 (s, 1H), 7.58 (s, 1H), 7.39 (s, 1H), 7.29 (d, J = 2.8 Hz, 3H), 7.27−7.22 (m, 2H), 5.36 (s, 2H), 3.50 (s, 2H), 2.94 (s, 4H), 2.52 (s, 4H). ^{13}C NMR (126 MHz, $CDCl_3$) δ 162.40, 153.51, 150.80, 143.08, 137.98, 135.23, 129.20, 128.21, 127.10, 69.42, 63.03, 52.94, 50.51; HRMS $[M + 1]^+$ calcd 456.1216, found 456.1227; HPLC purity: 96.84%; retention time: 3.4 min.

*4.1.4.16. 3-((4-Benzylpiperazin-1-yl)methyl)-5-(2-bromophenyl)-1,3,4-oxadiazole-2(3H)-thione (**SD-16**).* Light yellow solid, yield 70%, mp 226−228 °C; TLC (EtOAc/hexane, 80:20 v/v); R_f = 0.62. FT-IR (α ATR, ν cm^{-1}): 3065 (Ar−CH), 2938 (CH methylene) 1256 (C═S), 1640 (C═N); ^{1}H NMR (500 MHz, $CDCl_3$) δ 7.96 (dd, J = 8.1, 5.6 Hz, 2H), 7.52−7.48 (m, 2H), 7.31 (d, J = 4.4 Hz, 4H), 7.15 (s, 1H), 5.30 (s, 2H), 3.52 (s, 2H), 2.97 (s, 4H), 2.53 (s, 4H). ^{13}C NMR (126 MHz, $CDCl_3$) δ 164.73, 147.42, 139.24, 130.73, 129.30, 128.77, 128.51, 128.21, 127.10, 123.51, 69.54, 63.10, 53.06, 50.44; HRMS $[M + 1]^+$ calcd 444.0619, found 444.0624; HPLC purity: 95.54%; retention time: 3.7 min.

*4.1.4.17. 3-((4-Benzylpiperazin-1-yl)methyl)-5-(2,4-dihydroxyphenyl)-1,3,4-oxadiazole-2(3H)-thione (**SD-17**).* Yellow solid, yield 67%, mp 219−221 °C; TLC (EtOAc/hexane, 80:20 v/v); R_f = 0.48. FT-IR (α ATR, ν cm^{-1}): 3126 (Ar−CH), 2927 (CH methylene) 1245 (C═S), 1650 (C═N); ^{1}H NMR (500 MHz, DMSO) δ 9.56 (s, 2H), 8.62−8.53 (t, J = 7.1 Hz, 1H), 8.09−8.08 (d, J = 5.6 Hz, 1H), 7.69−7.60 (m, 1H), 7.34−7.31 (d, J = 9.7 Hz, 5H), 5.05 (s, 2H), 3.67 (s, 2H), 2.84 (s, 4H), 2.58 (d, J = 4.52 Hz, 4H). ^{13}C NMR (126 MHz, $CDCl_3$) δ 178.27, 158.91, 136.70, 134.77, 132.35, 129.16, 129.15, 128.91, 126.52, 122.46, 70.35, 62.74, 52.87, 50.23; HRMS $[M + 1]^+$ calcd 398.1413, found 398.1428; HPLC purity: 95.12%; retention time: 4.2 min.

4.2. Pharmacology. *4.2.1. In Vitro Cholinesterase (hAChE and hBChE) Inhibition Assay.* Designed compounds (**SD-1**−**17**) were assessed for their ability to inhibit both the cholinesterase enzymes (hAChE and hBChE) as per the Ellman protocol with certain modifications in the protocol.[47] The ChE enzyme preferentially hydrolyzes thiolated substrates into thiocholine that reduces 5,5-dithio-bis-(2-nitrobenzoic acid) (DTNB) and results in the production of a yellow color product, which is further measured colorimetrically at λ = 412 nm. All of the synthesized derivatives and standard drugs were initially dissolved using DMSO to prepare a stock solution, and from this five dilutions of different concentrations (increasing concentrations) were prepared in the phosphate-buffered saline (PBS). The hAChE (human erythrocytes) and hBChE (equine serum) enzymes were purchased from Sigma-Aldrich India. A final concentration of 0.22 U/mL solution of hAChE was used in the assay and was prepared using Tris buffer (pH 8). The assay was started in 96-well plates with the initial incubation of 50 μL of hAChE (0.22 U/mL) and 10 μL of inhibitors and standard solution for 30 min at room temp. Afterward, 30 μL of ATCI (1.5 mM in PBS) was added to each corresponding well with a further incubation of 30 min at room temperature. Finally, 160 μL of DTNB (0.15 mM) was added to each well, and absorbance was recorded immediately at λ = 412 nm on a 96-well microplate reader (Synergy HT, Bio-Tek Instruments, Inc.). The above-mentioned method with the same procedure was used to carry out the *in vitro* BChE assay with a slight alteration in the concentration of hBChE, BTCI, and DTNB (0.06 U/mL, 15 mM, and 1.5 mM, respectively); however, the concentration of the inhibitors and standards remained constant. The above-described experiments were carried out in triplicate (n = 3), and the results obtained were presented as mean ± SEM of the corresponding data. Utilizing all of the components used in the ChE assay except the enzyme, a blank solution was also prepared. The following expression was used to calculate the percentage inhibition: $[(Ac - Ai)/Ac] \times 100$, where Ai = absorbance with an inhibitor, while Ac = absorbance without an inhibitor. The IC_{50} value of each inhibitor/standard (for comparison of the data) used in the experiment was estimated using Graph Pad Prism 5.01.[47,50]

4.2.2. AChE Enzyme Kinetics. The mechanism of hAChE-catalyzed inhibition by the most effective compound **SD-6**, an enzyme kinetics investigation, was conducted. The kinetic parameters K_m and V_{max} were derived using a fixed concentration of enzyme against six different concentrations of ATCI (50−500 μM). Three different concentrations (0.03, 0.15, and 0.30 mM) of compound **SD-6** were used and evaluated against six different ATCI concentrations. The Michaelis−Menten nonlinear regression kinetics and Lineweaver−Burk plots were utilized to find V_{max} and K_m, and the mechanism of enzyme inhibition was determined by these plots.[51] Further, the respective K_i value was determined using a Dixon plot.[52] The experiment was conducted in triplicate (n = 3).

4.2.3. In Vitro hBACE-1 Inhibition Assay. A fluorescence resonance energy-transfer (FRET)-based analysis of BACE-1 enzymatic activity was determined using a human BACE-1 enzyme (Sigma-Aldrich) detection kit provided with a human BACE-1 enzyme, a BACE-1 substrate, a stop solution, a fluorescent assay buffer, and an assay standard. The assay was performed following the manufacturer's protocol, and the increased fluorescence intensity as a result of the breaking of the substrate in the presence of enzyme was measured. The enzyme inhibition potential of the compounds was estimated using different concentrations (showing 20−80% inhibition) and recorded on a multimode microplate reader at wavelengths λ = 320 and 405 nm as excitation and emission wavelengths, respectively.[25,30] The fluorescence intensity was monitored immediately after the addition of the BACE-1 enzyme, and the plates were further incubated for 2 h at 37 °C. After incubation, the fluorescence intensity was again recorded and the % enzyme inhibition was calculated using $[(IF_o - IF_i)/IF_o]$

https://doi.org/10.1021/acsomega.2c08061
ACS Omega 2023, 8, 9394−9414

× 100 (where IF_i = fluorescence intensity in the presence of inhibitor and IF_o = fluorescence intensity in the absence of inhibitor). A linear regression graph was plotted (Graph Pad Prism 5.01) to determine the IC_{50} values of each inhibitor molecule.

4.2.4. Propidium Iodide Displacement Assay. Propidium iodide (PI) tends to attach the PAS region of the AChE enzyme, and its specific inhibitor competes to displace the PI. The capability of the compounds to displace PI from the hAChE-PAS region was evaluated using the PI displacement assay. The hAChE enzymatic solution (5 U) was prepared in tris buffer (pH 8.0). Targeted compounds with various concentrations were added to the solution and incubated for 6 h at 25 °C. After incubation, PI was added, and after 10 min, fluorescence was examined at λ = 535 nm (excitation) and 595 nm (emission) wavelengths.

4.2.5. PAMPA−BBB Assay. The targeted compounds were analyzed to evaluate their *in vitro* BBB permeability *via* a PAMPA−BBB assay. The assay was performed on the PAMPA−BBB kit (KRISHGEN Biosystem) provided with 96-well acceptor and donor plates, dodecane, and dried brain lipid (DBL). The assay was performed as per the manufacturer's protocol. The donor plate with a porous bottom filter was coated with DBL (4 μL of 20 mg/mL in dodecane). The stock solution of both the test compounds was prepared in DMSO and further diluted with PBS pH 7.4 to make a final concentration of 25 μg/mL (DMSO ≤1%). The test compounds were first dissolved in DMSO; then, PBS pH 7.4 was added to produce the final dilution of 25 μg/mL. A fixed amount (200 μL) of test compounds and PBS pH 7.4 was added to the donor and acceptor plates, respectively, and both the plates were sandwiched together and incubated for 18 h at 37 °C to allow the entry of test compounds from the acceptor to the donor plate *via* the DBL membrane.[43] Following incubation, spectrophotometric analysis was used to quantify the drug concentrations in both plates. The experiment was carried out in triplicate (n = 3).

4.2.6. SH-SY5Y Neurotoxicity Estimation. The neuronal cells (SH-SY5Y) were grown in a neuronal induction medium (NIM) consisting of minimum essential medium (MEM) 5% fetal bovine serum (FBS) supplemented with 10 μM retinoic acid (RA). The cells were grown in the NIM medium for 6 days and then switched to serum-free NIM. The cytotoxic potential of compounds **SD-4** and **SD-6** was assessed on day 7 on differentiated SH-SY5Y cells using MTT assay. Cells (1×10^3 cells/well) were seeded in 96-well plates. After 24 h at 37 °C, culture media was removed and different concentrations (10, 20, 40, and 80 μM) of compounds **SD-4** and **SD-6** and donepezil were added and incubated further for 24 h at 37 °C. Further, 20 μL of MTT solution (0.5 mg/mL) was added to each well and incubated for 4 h at 37 °C. After 4 h, the medium was removed and DMSO (200 μL) was added; the formation of formazan crystals was observed, and absorbance was taken at 570 nm. Results have been represented as the mean ± standard deviation (SD) of three independent experiments (n = 3).[44,53,54]

4.2.7. SH-SY5Y Neuroprotective Estimation. The hydrogen peroxide (H_2O_2)-induced neuroprotective action of the compounds on nondifferentiated SH-SY5Y cells was examined by the MTT assay. A sufficient number of SH-SY5Y cells (2×10^4) were seeded in 96-well plates and incubated for 24 h at 37 °C. The different concentrations of the test compounds were added to 960-well plates containing cells and incubated further for 3 h at 37 °C. Afterward, H_2O_2 (200 μM) was added to each well and the plate was subjected to further incubation for 24 h at 37 °C. The positive control was prepared by cells treated with H_2O_2 only while the healthy control was prepared using the cells without treatment. The experiment was performed in triplicate (n = 3), and the results are expressed as the change in cell morphology and the population as mean ± SD, compared to positive and healthy control.[44]

4.2.8. Aβ-Aggregation Inhibition (Self- and AChE-Induced) Thioflavin T Assay. The self- and AChE-induced $A\beta_{1-42}$ aggregation inhibitory activities of compounds **SD-4** and **SD-6** were estimated using a thioflavin T (ThT) assay.[55,56] To the glass vial containing $A\beta_{1-42}$ (Caymann), 1% v/v of ammonium hydroxide pH ≥ 9.0 (sufficient quantity) was added to get a final concentration of 2000 μM as a stock solution and was stored at −80 °C. The further dilutions of $A\beta_{1-42}$ from stock solution were prepared in DMSO (molecular biology grade, Sigma-Aldrich) and PBS pH 7.4 (% DMSO ≤ 1% w/v). To initiate a self-induced $A\beta_{1-42}$ aggregation inhibition experiment, a fixed concentration of $A\beta_{1-42}$ (10 μM, 10 μL) was incubated with and without test compounds (5, 10, and 20 μM; 10 μL) in equal volume to that of $A\beta_{1-42}$ for 48 h at 37 °C. Using PBS pH 7.4 only in the presence and absence of inhibitors, a blank test run was performed. After incubation, the thioflavin T (5 μM in 50 mM glycine−NaOH buffer pH 8) was added to each mixture, and the fluorescence intensities were determined at λ = 485 and 528 nm, as excitation and emission wavelengths, respectively. The % anti-$A\beta_{1-42}$ potential of the test compounds was calculated using the expression $(IF_c - IF_i/IF_c) \times 100$, where IF_i = fluorescence intensity in the presence of inhibitors and IF_c = fluorescence intensity in the absence of inhibitors. The hAChE-induced anti-$A\beta_{1-42}$ aggregation experiment was performed in a similar way to that of the self-induced experiment with the only modification where a mixture of $A\beta_{1-42}$ (10 μM, 4 μL) and hAChE (230 μM, 16 μL) was taken instead of $A\beta_{1-42}$ only.[57] The results of hAChE-induced experiments are also determined and expressed in a manner similar to the self-induced protocol. Both experiments are conducted in triplicate (n = 3).

4.3. *In Vivo* Behavioral Studies. *4.3.1. Animals.* The Wistar rats of both the sex and having weights of 220−280 g per animal were procured from the authorized vendor of the institute. After receiving the animals, they were kept in a quarantine area for 14 days with a supply of normal water, a balanced diet, light/dark cycles for 12 h at temperature (25 ± 2 °C), and humidity (55 ± 10%). The animals were divided and segregated into a group of six. The Committee on Institutional Animal Ethics (Dean/2017/CAEC/93) has approved the study protocol.

4.3.2. Acute Toxicity Studies. Compound **SD-6**, with the highest inhibitory potential (*in vitro* findings), was tested according to the OECD-423 guidelines for any acute oral toxicity. The female Wistar rats (five animals in the group) fasted overnight before the study were given free access to water only. Compound **SD-6** was suspended in a vehicle, *i.e.*, 0.3% w/v of sodium carboxymethyl cellulose (Na-CMC), and this suspension was administered orally in divided doses of 100−500 mg/kg to the animals. The animals were also regularly monitored for any abnormal behavior and toxic reactions such as diarrhea, lethargy, *etc.*, for up to 14 days. After the study, the blood samples were collected and the animals

https://doi.org/10.1021/acsomega.2c08061
ACS Omega 2023, 8, 9394−9414

were sacrificed to perform a histopathological examination of various organs such as the brain, liver, and kidney.[58]

4.3.3. Scopolamine-Induced Amnesia Rat Model for Cognition Enhancement Testing. The scopolamine hydrobromide was dissolved in sterile normal saline to prepare the stock solution. The suspension of donepezil and test compound **SD-6** was prepared in Na-CMC, 0.3% w/v. The experimental animals (n = 6) were divided into six groups control, scopolamine, donepezil, and **SD-6** 2.5, 5, and 10 mg/kg groups. For 7 days, the animal groups received oral doses of donepezil and **SD-6** suspension. Only 0.3% of Na-CMC vehicle was administered to the scopolamine group rats.

4.3.4. Scopolamine-Induced Y-Maze Test. The scopolamine hydrobromide in normal saline was administered intraperitoneally to each treated group after the 7th day of the treatment except the control group. The improvement in an instant and short-term memory was analyzed through the Y-maze test. The maze comprised three arms of Y-shaped. The rats were independently positioned in the maze's middle. The initial entry was eliminated from the calculations because the rats would frequently enter the arm of facing. The animals were observed carefully for about 8 min for total arm entries and also watched for spontaneous alternations.[59] The results of the Y-maze experiment are expressed using the following equation: percent spontaneous alteration = [number of spontaneous alternations/(total arm entries-2)] × 100 has been utilized for memory improvement score.[60]

4.3.5. Aβ-Induced Morris Water Maze Test. In the $A\beta_{1-42}$-induced ICV rat model, the four groups of animals (control, sham, donepezil, and **SD-6**) of adult male Wistar rats weighing 220−280 g, having six animals in each group, were used. The sterile 0.9% of NaCl solution was used as the vehicle and also used to dissolve the $A\beta_{1-42}$ (Sigma-Aldrich, India). The ketamine (90 mg/kg, i.p.) in combination with the xylazine (9 mg/kg, i.p.) cocktail was used for anesthesia. The rats, post anesthesia, were kept on the stereotaxic equipment after cleaning their scalp with iodine solution, and saline and ear bars were set symmetrically. The skull of the rat brain was drilled using stereotaxic coordinates bregma (−0.5 mm anteroposterior, −3.2 mm dorsoventral with an incision bar set at −3.3 mm and +1.2 mm mediolateral) to put a hole in it.[61] With the exception of the sham group, all of the rats received $A\beta_{1-42}$ (4 μM, 5 μL) injections with a 2 μL/min infusion rate using a Hamilton microsyringe. However, the sham group received only a vehicle. Following a 7 day period of postoperative recuperation, donepezil (5 mg/kg) and **SD-6** (10 mg/kg) were given orally to each respective group of animals on the eighth day for a total of nine consecutive days, *i.e.*, up to the 16th day. During the last 5 days of treatment (12−16th days), the Morris water maze test was performed to determine learning and memory improvements in the experimental animals. The Morris water maze comprised a circular pool (diameter 121 cm, depth 32 cm, and height 62 cm) filled with water (25 ± 2 °C). The pool was made opaque using TiO_2 to hide the platform 2 cm under the water surface and divided into four equal quadrants. The number of platform crossings and the escape latency time was determined for a period of 90 s, two trials every day with a minimum of 3 h difference.[62]

4.3.6. Ex Vivo Biochemical Estimation. The animals from each group after behavioral studies were sacrificed, and their brains were isolated carefully. The hippocampal region of the rat brains was again separated and further subjected to homogenization in cold PBS, pH 7.4. The brain homogenates were finally centrifuged at 4 °C for 10 min, and the supernatant was used for various *ex vivo* biochemical estimations.

The hippocampal AChE level in rat brains was estimated using a modified Ellman colorimetric method. The supernatant after centrifugation (50 μL) was preincubated with ATCI (15 mM, 100 μL) for 30 min, followed by the addition of DTNB solution (1.5 mM, 100 μL) to the mixture at 37 °C, and the absorbance was measured at the wavelength (λ = 412 nm) for 6 min to determine the rate of change in the enzymatic reaction. The results are calculated as the ATCI hydrolysis μM of substrate hydrolyzed/min/mg of protein of three independent experiments.

The estimation of the ACh in the brain homogenate was performed as per the manufacturer's instruction (Krishgen Biosystems, rat acetylcholine, ACH GENLISA ELISA) on an ELISA kit, and the amount of ACh was expressed as pg/mL.

The presence of MDA level in the hippocampal brain was estimated to check the antioxidant potential of the compound. The TBARS assay (lipid peroxidation assay) was performed, which involved the detection of MDA and thiobarbituric acid complex TBARS (red color) in an acidic solution. To estimate the levels of MDA in the rat brain, a supernatant of 200 μL was mixed with 1 mL of 10% v/v trichloroacetic acid in 0.1 M of HCl and centrifuged for 10 min at 4 °C. Equal proportions of the supernatants so obtained and thiobarbituric acid (0.67%) were warmed for 10 min in a water bath, and the absorbance of the mixture was recorded at the wavelength (λ = 532 nm) after attaining the normal temperature. The results are expressed as the number of moles of MDA/mg of protein in the three independent experiments.[63]

The SOD assay was performed to assess the antioxidant potential of the compound. The assay performed was based on the formation of blue color formazan as a result of autoxidation of hydroxylamine hydrochloride (pH 10.2) by SOD (free-radical dismutation enzyme) in the presence of ethylenediaminetetraacetic acid (EDTA). Equal proportions (50 μL) of each of the brain homogenate (hippocampal) and the hydroxylamine hydrochloride were added to a mixture containing EDTA (100 μM), Na_2CO_3 (50 mM), and the nitro blue tetrazolium (24 μM). After addition, the absorbance was recorded at λ = 560 nm wavelength, and results are represented as SOD units (U/mL)/min/mg of protein of three independent experiments.[64]

Reduced glutathione (GSH) assay was conducted by mixing 100 μL of supernatant from hippocampal brain tissue homogenate and 1 mL of 4% w/v sulfosalicylic acid. The precipitate formed after mixing was kept at a temperature of 2−8 °C in a refrigerator for 1 h. The cold precipitate was centrifuged after 1 h in a cold centrifuge (1200g for 15 min at 4 °C). After centrifugation, the pellet obtained was discarded and the supernatant was utilized further in the next step. The supernatant of 100 μL was diluted with 2.7 mL of 0.1 M PBS (pH 8), and to this, 200 μL of 0.1 M DTNB (Ellman's reagent) solution was added, which resulted in a pale yellow color solution, and the absorbance was recorded at λ = 412 nm on a multimode microplate reader (Synergy HT, Bio-Tek Instruments, Inc.). Furthermore, by using the molar extinct coefficient of 1.36×10^4 M^{-1} cm^{-1}, the calculation was performed and expressed as nmol GSH per mg of protein.[65]

The catalase assay was done by mixing 50 μL of supernatant from the brain hippocampal tissue and 3 mL of H_2O_2−phosphate buffer (12.5 mM H_2O_2 in 50 mM phosphate buffer

https://doi.org/10.1021/acsomega.2c08061
ACS Omega 2023, 8, 9394−9414

and adjusted pH 7.0). The absorbance was recorded immediately after adding H_2O_2 at λ = 240 nm for 2 min in each 60 sec time interval, and the results are expressed as μmol of H_2O_2 decomposed/min/mg of protein.[66]

4.3.7. Animal Tissue Histopathology. For performing the histopathology of the brain tissues of rats, the rats were sacrificed after transcardial perfusion with precooled PBS pH 7.4 followed by 4% formaldehyde (in 0.1 mol/L PBS). The brains from each group were isolated and kept at 4 °C overnight for fixation. The brains were transferred to a container of 10%, followed by 20 and 40% sucrose solutions (24 h with each sucrose solution) for complete dehydration. The brain blocks were prepared, and the sectioning of the brain was done using a freezing microtome (Leica Microsystems, Germany) and collected in 0.01 mol/L of PBS and washed thrice. The free-floating brain sections were mounted on the glass slides, and Nissl's staining (0.125% cresyl violet) was applied to the section, followed by washing with alcohol (70, 95, and 100%) and with xylene thrice. Finally, the images were captured in a light microscope (MLXi-TR plus from Olympus) and Nissl's stained neurons were counted (neuronal density) using ImageJ software and expressed as % of control rats.[67]

4.4. *In Silico* Studies. *4.4.1. Molecular Dockings.* The molecular docking studies of compounds **SD-4** and **SD-6** were performed against hAChE (PDB Code: 4EY7), hBChE (PDB code: 4TPK), and hBACE-1 (PDB Code: 2ZJM) to examine the binding of the ligands in the active site of the proteins. Schrodinger Maestro 2018-1 software was used to perform molecular dockings. Schrodinger's protein preparation wizard module was used to process and prepare the protein, such as to add hydrogen atoms; the force field OPLS-2005 was used to allocate the partial charges, and by using the Prime module of the Schrodinger, the missing side chains and loops were added. Epik was used at pH 7.0 to create heteroatom states, and the water molecules larger than 5 Å were removed from the heteroatoms. Additionally, the PROPKA technique at pH 7.0 was used to minimize the structure of the protein by keeping the convergence threshold RMSD of the atoms at 0.30 Å at constrained minimization. Using the Grid generation program, an active site of 10 × 10 × 10 $Å^3$ was created around the centric cocrystallized ligand (donepezil for hAChE, rivastigmine for hBChE, and F1M for hBACE-1) in the cocrystallized protein structure. The stable confirmations of compounds **SD-4** and **SD-6** were generated using the LigPrep module of the Schrodinger Maestro 2018-1, and these stable confirmations of both the compounds were docked against the three enzymes using the Glide module of Schrodinger Maestro 2018-1. Finally, the XP visualizer tool was used to estimate the binding interactions of the compounds in the active site of hAChE, hBChE, and BACE-1 enzymes.[68]

4.4.2. Molecular Dynamics. Desmond was used to affirm the binding stability of the ligand−protein complex of compounds **SD-4** and **SD-6** with hAChE, hBChE, and hBACE-1, and the MD simulation experiments of 100 ns were performed using their respective docked poses. The docked complexes were first immersed and soaked in TIP3P water molecules enclosed in the cubic water box to produce the clear-cut water environment. The counterions were added to neutralize the water system, and the isotonicity of this water system was maintained by adding 0.15 M of NaCl. The system energy of the complex was minimized by 1 kcal/mol/Å of convergence criteria by combining a gradient approach with a maximum of 2000 interactions. After achieving energy minimization, an MD simulation run of the complex for 100 ns in an isothermal−isobaric ensemble (NPT) was conducted with periodic boundary conditions. The predefined temperature (300 K) and pressure (1013 atmospheric bars) were adjusted throughout the run of 100 ns.[69]

4.4.3. In Silico Determination of Drug-Like Properties. The drug-likeness properties of the compounds were identified using the QikProp module of the Schrodinger Maestro's 2018-1. Lipinski's rule of five (donor HB <5, accept HB <10, mol MW <500, QPlog Po/w <5) was used to predict a number of descriptors, including QPlogBB, solvent-accessible surface area (SASA), and others, to assess the drug-likeness properties in the compounds.[70]

4.4.4. Binding Free-Energy (MM/GBSA) Calculation. The binding free energy (ΔG_{bind}) was calculated as an average of several protein−ligand confirmations. The binding free energy of the protein−ligand complex was calculated based on the $\Delta G_{bind} = G_{complex} - G_{protein} - G_{ligand}$, where G_{bind}, $G_{complex}$, $G_{protein}$, and G_{ligand} are the binding free energy, free energy for complex, free energy for protein, and free energy for ligand, respectively. The energies were estimated using the equation $\Delta E_{MM} + \Delta G_{GB} + \Delta G_{nonpolar} - T\Delta S$ (ΔE_{MM} = gas-phase interaction, ΔG_{GB}, $\Delta G_{nonpolar}$ = polar and nonpolar components of the desolvation, and $T\Delta S$ is the change in conformational entropy). The prime MM/GBSA module of Schrödinger 2018-1 was used to calculate the ΔG_{bind} of the docked complexes of **SD-4** and **SD-6** against hAChE, hBChE, and hBACE-1. The results of MM/GBSA are expressed as ΔG_{bind} in kcal/mol for both the compounds and standards.[71]

■ ASSOCIATED CONTENT

Supporting Information

The Supporting Information is available free of charge at https://pubs.acs.org/doi/10.1021/acsomega.2c08061.

SAR, computational, biological, and analytical characterization data of the compounds such as ^{1}H NMR, ^{13}C NMR, FT-IR, mass spectra, and HPLC purity chromatograms (PDF)

■ AUTHOR INFORMATION

Corresponding Author

Sushant Kumar Shrivastava − *Pharmaceutical Chemistry Research Laboratory, Department of Pharmaceutical Engineering and Technology, Indian Institute of Technology-Banaras Hindu University, Varanasi 221005, India;* orcid.org/0000-0002-5500-4004; Email: skshrivastava.phe@itbhu.ac.in

Authors

Digambar Kumar Waiker − *Pharmaceutical Chemistry Research Laboratory, Department of Pharmaceutical Engineering and Technology, Indian Institute of Technology-Banaras Hindu University, Varanasi 221005, India*

Akash Verma − *Pharmaceutical Chemistry Research Laboratory, Department of Pharmaceutical Engineering and Technology, Indian Institute of Technology-Banaras Hindu University, Varanasi 221005, India*

Poorvi Saraf − *Pharmaceutical Chemistry Research Laboratory, Department of Pharmaceutical Engineering and Technology, Indian Institute of Technology-Banaras Hindu University, Varanasi 221005, India*

https://doi.org/10.1021/acsomega.2c08061
ACS Omega 2023, 8, 9394−9414

Gajendra T.A. − *Neurotherapeutics Research Laboratory, Department of Pharmaceutical Engineering and Technology, Indian Institute of Technology-Banaras Hindu University, Varanasi 221005, India*

Sairam Krishnamurthy − *Neurotherapeutics Research Laboratory, Department of Pharmaceutical Engineering and Technology, Indian Institute of Technology-Banaras Hindu University, Varanasi 221005, India*

Rameshwar Nath Chaurasia − *Institute of Medical Sciences, Faculty of Medicine, Department of Neurology, Banaras Hindu University, Varanasi 221005, India*

Complete contact information is available at: https://pubs.acs.org/10.1021/acsomega.2c08061

Notes

The authors declare no competing financial interest.

■ ACKNOWLEDGMENTS

The authors would like to thank the Central Instrumentation Facility (CIF), Indian Institute of Technology-Banaras Hindu University (IIT-BHU), Varanasi, for the NMR facility. D.K.W. would like to thank SERB for financial support (SERB CRG project) file no. CRG/2021/005651.

■ REFERENCES

(1) DeTure, M. A.; Dickson, D. W. The neuropathological diagnosis of Alzheimer's disease. *Mol. Neurodegener.* **2019**, *14*, No. 32.

(2) Srivastava, S.; Ahmad, R.; Khare, S. K. Alzheimer's disease and its treatment by different approaches: A review. *Eur. J. Med. Chem.* **2021**, *216*, No. 113320.

(3) Gauthier, S.; Rosa-Neto, P.; Morais, J.; Webster, C. *World Alzheimer Report: Journey through the Diagnosis of Dementia*; Alzheimer's Disease International, 2021.

(4) Patterson, C. *World Alzheimer Report*; Alzheimer's Disease International, 2018.

(5) Nandi, A.; Counts, N.; Chen, S.; Seligman, B.; Tortorice, D.; Vigo, D.; Bloom, D. E. Global and regional projections of the economic burden of Alzheimer's disease and related dementias from 2019 to 2050: A value of statistical life approach. *eClinicalMedicine* **2022**, *51*, No. 101580.

(6) Li, H.; Li, Y.; Liang, W.; Wei, Z. Z.; Li, X.; Tian, Y.; Qiao, S.; Yang, Y.; Yang, L.; Wu, D.; et al. The identification of PSEN1 p. Tyr159Ser mutation in a non-canonic early-onset Alzheimer's disease family. *Mol. Cell. Neurosci.* **2022**, *120*, No. 103715.

(7) Petit, D.; Fernández, S. G.; Zoltowska, K. M.; Enzlein, T.; Ryan, N. S.; O'Connor, A.; Szaruga, M.; Hill, E.; Vandenberghe, R.; Fox, N. C.; Chávez-Gutiérrez, L. Aβ profiles generated by Alzheimer's disease causing PSEN1 variants determine the pathogenicity of the mutation and predict age at disease onset. *Mol. Psychiatry* **2022**, *27*, 2821−2832.

(8) Oumata, N.; Lu, K.; Teng, Y.; Cavé, C.; Peng, Y.; Galons, H.; Roques, B. P. Molecular mechanisms in Alzheimer's disease and related potential treatments such as structural target convergence of antibodies and simple organic molecules. *Eur. J. Med. Chem.* **2022**, *240*, No. 114578.

(9) Dorszewska, J.; Prendecki, M.; Oczkowska, A.; Dezor, M.; Kozubski, W. Molecular basis of familial and sporadic Alzheimer's disease. *Curr. Alzheimer Res.* **2016**, *13*, 952−963.

(10) Hensley, K.; Carney, J.; Mattson, M.; Aksenova, M.; Harris, M.; Wu, J.; Floyd, R.; Butterfield, D. A model for beta-amyloid aggregation and neurotoxicity based on free radical generation by the peptide: relevance to Alzheimer disease. *Proc. Natl. Acad. Sci. U.S.A.* **1994**, *91*, 3270−3274.

(11) Enz, A. Acetylcholinesterase Inhibitors (AChE-I) as a Potential Use for Alzheimer's Disease (AD) Therapy. *Enzymes of the Cholinesterase Family*; Springer, 1995; pp 475−476.

(12) Hynd, M. R.; Scott, H. L.; Dodd, P. R. Glutamate-mediated excitotoxicity and neurodegeneration in Alzheimer's disease. *Neurochem. Int.* **2004**, *45*, 583−595.

(13) Heneka, M. T.; Carson, M. J.; El Khoury, J.; Landreth, G. E.; Brosseron, F.; Feinstein, D. L.; Jacobs, A. H.; Wyss-Coray, T.; Vitorica, J.; Ransohoff, R. M.; et al. Neuroinflammation in Alzheimer's disease. *Lancet Neurol.* **2015**, *14*, 388−405.

(14) Alonso, A. d. C.; Grundke-Iqbal, I.; Iqbal, K. Alzheimer's disease hyperphosphorylated tau sequesters normal tau into tangles of filaments and disassembles microtubules. *Nat. Med.* **1996**, *2*, 783−787.

(15) Markesbery, W. R. Oxidative stress hypothesis in Alzheimer's disease. *Free Radical Biol. Med.* **1997**, *23*, 134−147.

(16) Kaide, S.; Watanabe, H.; Shimizu, Y.; Tatsumi, H.; Iikuni, S.; Nakamoto, Y.; Togashi, K.; Ihara, M.; Saji, H.; Ono, M. 18F-labeled benzimidazopyridine derivatives for PET imaging of tau pathology in Alzheimer's disease. *Bioorg. Med. Chem.* **2019**, *27*, 3587−3594.

(17) Zemek, F.; Drtinova, L.; Nepovimova, E.; Sepsova, V.; Korabecny, J.; Klimes, J.; Kuca, K. Outcomes of Alzheimer's disease therapy with acetylcholinesterase inhibitors and memantine. *Expert Opin. Drug Saf.* **2014**, *13*, 759−774.

(18) Yang, P.; Sun, F. Aducanumab: The first targeted Alzheimer's therapy. *Drug Discovery Ther.* **2021**, *15*, 166−168.

(19) Rivera-Marrero, S.; Bencomo-Martínez, A.; Salazar, E. O.; Sablón-Carrazana, M.; García-Pupo, L.; Zoppolo, F.; Arredondo, F.; Dapueto, R.; Santi, M. D.; Kreimerman, I.; et al. A new naphthalene derivative with anti-amyloidogenic activity as potential therapeutic agent for Alzheimer's disease. *Bioorg. Med. Chem.* **2020**, *28*, No. 115700.

(20) Talesa, V. N. Acetylcholinesterase in Alzheimer's disease. *Mech. Ageing Dev.* **2001**, *122*, 1961−1969.

(21) Huang, Y.; Mucke, L. Alzheimer mechanisms and therapeutic strategies. *Cell* **2012**, *148*, 1204−1222.

(22) Stanciu, G. D.; Luca, A.; Rusu, R. N.; Bild, V.; Beschea Chiriac, S. I.; Solcan, C.; Bild, W.; Ababei, D. C. Alzheimer's disease pharmacotherapy in relation to cholinergic system involvement. *Biomolecules* **2020**, *10*, No. 40.

(23) Mushtaq, G.; Greig, N.; Khan, J.; Kamal, M. Status of acetylcholinesterase and butyrylcholinesterase in Alzheimer's disease and type 2 diabetes mellitus. *CNS Neurol. Disord.: Drug Targets* **2014**, *13*, 1432−1439.

(24) Mao, P.; Reddy, P. H. Aging and amyloid beta-induced oxidative DNA damage and mitochondrial dysfunction in Alzheimer's disease: implications for early intervention and therapeutics. *Biochim. Biophys. Acta, Mol. Basis Dis.* **2011**, *1812*, 1359−1370.

(25) Sharma, P.; Tripathi, A.; Tripathi, P. N.; Prajapati, S. K.; Seth, A.; Tripathi, M. K.; Srivastava, P.; Tiwari, V.; Krishnamurthy, S.; Shrivastava, S. K. Design and development of multitarget-directed N-Benzylpiperidine analogs as potential candidates for the treatment of Alzheimer's disease. *Eur. J. Med. Chem.* **2019**, *167*, 510−524.

(26) Sharma, P.; Tripathi, A.; Tripathi, P. N.; Singh, S. S.; Singh, S. P.; Shrivastava, S. K. Novel molecular hybrids of n-benzylpiperidine and 1, 3, 4-oxadiazole as multitargeted therapeutics to treat alzheimer's disease. *ACS Chem. Neurosci.* **2019**, *10*, 4361−4384.

(27) Tripathi, P. N.; Srivastava, P.; Sharma, P.; Seth, A.; Shrivastava, S. K. Design and development of novel N-(pyrimidin-2-yl)-1, 3, 4-oxadiazole hybrids to treat cognitive dysfunctions. *Bioorg. Med. Chem.* **2019**, *27*, 1327−1340.

(28) Hussein, W.; Sağlık, B. N.; Levent, S.; Korkut, B.; Ilgın, S.; Özkay, Y.; Kaplancıklı, Z. A. Synthesis and biological evaluation of new cholinesterase inhibitors for Alzheimer's disease. *Molecules* **2018**, *23*, No. 2033.

(29) Popugaeva, E.; Chernyuk, D.; Zhang, H.; Postnikova, T. Y.; Pats, K.; Fedorova, E.; Poroikov, V.; Zaitsev, A. V.; Bezprozvanny, I. Derivatives of piperazines as potential therapeutic agents for Alzheimer's disease. *Mol. Pharmacol.* **2019**, *95*, 337−348.

(30) Tripathi, A.; Choubey, P. K.; Sharma, P.; Seth, A.; Tripathi, P. N.; Tripathi, M. K.; Prajapati, S. K.; Krishnamurthy, S.; Shrivastava, S. K. Design and development of molecular hybrids of 2-pyridylpiper-

azine and 5-phenyl-1, 3, 4-oxadiazoles as potential multifunctional agents to treat Alzheimer's disease. *Eur. J. Med. Chem.* **2019**, *183*, No. 111707.
(31) Gutti, G.; Kakarla, R.; Kumar, D.; Beohar, M.; Ganeshpurkar, A.; Kumar, A.; Krishnamurthy, S.; Singh, S. K. Discovery of novel series of 2-substituted benzo [d] oxazol-5-amine derivatives as multi-target directed ligands for the treatment of Alzheimer's disease. *Eur. J. Med. Chem.* **2019**, *182*, No. 111613.
(32) Modh, R. P.; Kumar, S. P.; Jasrai, Y. T.; Chikhalia, K. H. Design, Synthesis, Biological Evaluation, and Molecular Modeling of Coumarin−P iperazine Derivatives as Acetylcholinesterase Inhibitors. *Arch. Pharm.* **2013**, *346*, 793−804.
(33) Shachar, D. B.; Kahana, N.; Kampel, V.; Warshawsky, A.; Youdim, M. B. Neuroprotection by a novel brain permeable iron chelator, VK-28, against 6-hydroxydopamine lession in rats. *Neuropharmacology* **2004**, *46*, 254−263.
(34) Li, D.; Li, J.; Huang, L. Protective effects of fenazinel dihydrochloride on focal cerebral ischemic injury in rats. *Chin. Pharmacol. Bull.* **2009**, *25*, 716−720.
(35) Saraf, P.; Tripathi, P. N.; Tripathi, M. K.; Tripathi, A.; Verma, H.; Waiker, D. K.; Singh, R.; Shrivastava, S. K. Novel 5, 6-diphenyl-1, 2, 4-triazine-3-thiol derivatives as dual COX-2/5-LOX inhibitors devoid of cardiotoxicity. *Bioorg. Chem.* **2022**, *129*, No. 106147.
(36) Muñoz-Ruiz, P.; Rubio, L.; García-Palomero, E.; Dorronsoro, I.; del Monte-Millán, M.; Valenzuela, R.; Usán, P.; de Austria, C.; Bartolini, M.; Andrisano, V.; et al. Design, synthesis, and biological evaluation of dual binding site acetylcholinesterase inhibitors: new disease-modifying agents for Alzheimer's disease. *J. Med. Chem.* **2005**, *48*, 7223−7233.
(37) Greig, N. H.; Utsuki, T.; Yu, Q.-s.; Zhu, X.; Holloway, H. W.; Perry, T.; Lee, B.; Ingram, D. K.; Lahiri, D. K. A new therapeutic target in Alzheimer's disease treatment: attention to butyrylcholinesterase. *Curr. Med. Res. Opin.* **2001**, *17*, 159−165.
(38) Verma, A.; Waiker, D. K.; Bhardwaj, B.; Saraf, P.; Shrivastava, S. K. The molecular mechanism, targets, and novel molecules in the treatment of Alzheimer's disease. *Bioorg. Chem.* **2021**, No. 105562.
(39) Rajmohan, R.; Reddy, P. H. Amyloid-beta and phosphorylated tau accumulations cause abnormalities at synapses of Alzheimer's disease neurons. *J. Alzheimer's Dis.* **2017**, *57*, 975−999.
(40) Cole, S. L.; Vassar, R. The Alzheimer's disease β-secretase enzyme, BACE1. *Mol. Neurodegener.* **2007**, *2*, 1−25.
(41) Silva, D.; Chioua, M.; Samadi, A.; Agostinho, P.; Garção, P.; Lajarín-Cuesta, R.; de Los Ríos, C.; Iriepa, I.; Moraleda, I.; Gonzalez-Lafuente, L.; et al. Synthesis, pharmacological assessment, and molecular modeling of acetylcholinesterase/butyrylcholinesterase inhibitors: effect against amyloid-β-induced neurotoxicity. *ACS Chem. Neurosci.* **2013**, *4*, 547−565.
(42) Pulicherla, K. K.; Verma, M. K. Targeting therapeutics across the blood brain barrier (BBB), prerequisite towards thrombolytic therapy for cerebrovascular disorders—an overview and advancements. *AAPS PharmSciTech* **2015**, *16*, 223−233.
(43) Di, L.; Kerns, E. H.; Fan, K.; McConnell, O. J.; Carter, G. T. High throughput artificial membrane permeability assay for blood−brain barrier. *Eur. J. Med. Chem.* **2003**, *38*, 223−232.
(44) Lingappa, S.; Shivakumar, M. S.; Manivasagam, T.; Somasundaram, S. T.; Seedevi, P. Neuroprotective Effect of Epalrestat on Hydrogen Peroxide-Induced Neurodegeneration in SH-SY5Y Cellular Model. *J. Microbiol. Biotechnol.* **2021**, *31*, 867−874.
(45) Wang, Z.; Wang, Y.; Wang, B.; Li, W.; Huang, L.; Li, X. Design, synthesis, and evaluation of orally available clioquinol-moracin M hybrids as multitarget-directed ligands for cognitive improvement in a rat model of neurodegeneration in Alzheimer's disease. *J. Med. Chem.* **2015**, *58*, 8616−8637.
(46) Klinkenberg, I.; Blokland, A. The validity of scopolamine as a pharmacological model for cognitive impairment: a review of animal behavioral studies. *Neurosci. Biobehav. Rev.* **2010**, *34*, 1307−1350.
(47) Ellman, G. L.; Courtney, K. D.; Andres, V., Jr.; Featherstone, R. M. A new and rapid colorimetric determination of acetylcholinesterase activity. *Biochem. Pharmacol.* **1961**, *7*, 88−95.
(48) Livani, Z. A.; Safakish, M.; Hajimahdi, Z.; Soleymani, S.; Zabihollahi, R.; Aghasadeghi, M. R.; Alipour, E.; Zarghi, A. Design, synthesis, molecular modeling, in silico ADME studies and anti-HIV-1 assay of new diazocoumarin derivatives. *Iran. J. Pharm. Res.* **2018**, *17*, 65.
(49) Al-Wahaibi, L. H.; Mohamed, A. A.; Tawfik, S. S.; Hassan, H. M.; El-Emam, A. A. 1, 3, 4-Oxadiazole N-Mannich bases: synthesis, antimicrobial, and anti-proliferative activities. *Molecules* **2021**, *26*, No. 2110.
(50) Singh, Y. P.; Tej, G. N. V. C.; Pandey, A.; Priya, K.; Pandey, P.; Shankar, G.; Nayak, P. K.; Rai, G.; Chittiboyina, A. G.; Doerksen, R. J.; et al. Design, synthesis and biological evaluation of novel naturally-inspired multifunctional molecules for the management of Alzheimer's disease. *Eur. J. Med. Chem.* **2020**, *198*, No. 112257.
(51) Lineweaver, H.; Burk, D. The determination of enzyme dissociation constants. *J. Am. Chem. Soc.* **1934**, *56*, 658−666.
(52) Dixon, M. The graphical determination of Km and Ki. *Biochem. J.* **1972**, *129*, 197−202.
(53) Mongre, R. K.; Mishra, C. B.; Jung, S.; Lee, B. S.; Quynh, N. T. N.; Anh, N. H.; Myagmarjav, D.; Jo, T.; Lee, M. S. Exploring the role of TRIP-Brs in human breast cancer: an investigation of expression, clinicopathological significance, and prognosis. *Mol. Ther.—Oncolytics* **2020**, *19*, 105−126.
(54) Mishra, C. B.; Mongre, R. K.; Prakash, A.; Jeon, R.; Supuran, C. T.; Lee, M.-S. Anti-breast cancer action of carbonic anhydrase IX inhibitor 4-[4-(4-Benzo [1, 3] dioxol-5-ylmethyl-piperazin-1-yl)-benzylidene-hydrazinocarbonyl]-benzenesulfonamide (BSM-0004): In vitro and in vivo studies. *J. Enzyme Inhib. Med. Chem.* **2021**, *36*, 954−963.
(55) Levine, H., III [18] Quantification of β-Sheet Amyloid Fibril Structures with Thioflavin T. *Methods in Enzymology*; Elsevier, 1999; pp 274−284.
(56) Levine, H., III Thioflavine T interaction with synthetic Alzheimer's disease β-amyloid peptides: Detection of amyloid aggregation in solution. *Protein Sci.* **1993**, *2*, 404−410.
(57) Bolognesi, M. L.; Cavalli, A.; Valgimigli, L.; Bartolini, M.; Rosini, M.; Andrisano, V.; Recanatini, M.; Melchiorre, C. Multi-target-directed drug design strategy: from a dual binding site acetylcholinesterase inhibitor to a trifunctional compound against Alzheimer's disease. *J. Med. Chem.* **2007**, *50*, 6446−6449.
(58) Lu, C.; Guo, Y.; Yan, J.; Luo, Z.; Luo, H.-B.; Yan, M.; Huang, L.; Li, X. Design, synthesis, and evaluation of multitarget-directed resveratrol derivatives for the treatment of Alzheimer's disease. *J. Med. Chem.* **2013**, *56*, 5843−5859.
(59) Wolf, A.; Bauer, B.; Abner, E. L.; Ashkenazy-Frolinger, T.; Hartz, A. M. A comprehensive behavioral test battery to assess learning and memory in 129S6/Tg2576 mice. *PLoS One* **2016**, *11*, No. e0147733.
(60) Jin, G.; Wang, L.-H.; Ji, X.-F.; Chi, T.-Y.; Qi, Y.; Jiao, Q.; Xu, Q.; Zhou, X.-Y.; Zhang, R.; Zou, L.-B. Xanthoceraside rescues learning and memory deficits through attenuating beta-amyloid deposition and tau hyperphosphorylation in APP mice. *Neurosci. Lett.* **2014**, *573*, 58−63.
(61) Colaianna, M.; Tucci, P.; Zotti, M.; Morgese, M. G.; Schiavone, S.; Govoni, S.; Cuomo, V.; Trabace, L. Soluble βamyloid1-42: a critical player in producing behavioural and biochemical changes evoking depressive-related state? *Br. J. Pharmacol.* **2010**, *159*, 1704−1715.
(62) Morris, R. Developments of a water-maze procedure for studying spatial learning in the rat. *J. Neurosci. Methods* **1984**, *11*, 47−60.
(63) Choubey, P. K.; Tripathi, A.; Tripathi, M. K.; Seth, A.; Shrivastava, S. K. Design, synthesis, and evaluation of N-benzylpyrrolidine and 1, 3, 4-oxadiazole as multitargeted hybrids for the treatment of Alzheimer's disease. *Bioorg. Chem.* **2021**, *111*, No. 104922.
(64) Tripathi, A.; Choubey, P. K.; Sharma, P.; Seth, A.; Saraf, P.; Shrivastava, S. K. Design, synthesis, and biological evaluation of ferulic acid based 1, 3, 4-oxadiazole hybrids as multifunctional therapeutics

https://doi.org/10.1021/acsomega.2c08061
ACS Omega 2023, 8, 9394−9414

for the treatment of Alzheimer's disease. *Bioorg. Chem.* **2020**, *95*, No. 103506.
(65) Jollow, D.; Mitchell, J.; Zampaglione, N.; Gillette, J. Bromobenzene-induced liver necrosis. Protective role of glutathione and evidence for 3, 4-bromobenzene oxide as the hepatotoxic metabolite. *Pharmacology* **1974**, *11*, 151−169.
(66) Akhtar, A.; Dhaliwal, J.; Saroj, P.; Uniyal, A.; Bishnoi, M.; Sah, S. P. Chromium picolinate attenuates cognitive deficit in ICV-STZ rat paradigm of sporadic Alzheimer's-like dementia via targeting neuroinflammatory and IRS-1/PI3K/AKT/GSK-3β pathway. *Inflammopharmacology* **2020**, *28*, 385−400.
(67) Mishra, A.; Krishnamurthy, S. Neurorestorative effects of subchronic administration of ambroxol in rodent model of Parkinson's disease. *Naunyn-Schmiedeberg's Arch. Pharmacol.* **2020**, *393*, 429−444.
(68) Shrivastava, S. K.; Nivrutti, A. A.; Bhardwaj, B.; Waiker, D. K.; Verma, A.; Tripathi, P. N.; Tripathi, M.; Saraf, P. Drug reposition-based design, synthesis, and biological evaluation of dual inhibitors of acetylcholinesterase and β-Secretase for treatment of Alzheimer's disease. *J. Mol. Struct.* **2022**, *1262*, No. 132979.
(69) Singh, U.; Laxmi; Singh, P.; Singh, A. K.; Singh, S.; Kumar, D.; Shrivastava, S. K.; Asthana, R. K. In silico and in vitro evaluation of extract derived from *Dunaliella salina*, a halotolerant microalga for its antifungal and antibacterial activity. *J. Biomol. Struct. Dyn.* **2022**, 1−15.
(70) Tripathi, M. K.; Sharma, P.; Tripathi, A.; Tripathi, P. N.; Srivastava, P.; Seth, A.; Shrivastava, S. K. Computational exploration and experimental validation to identify a dual inhibitor of cholinesterase and amyloid-beta for the treatment of Alzheimer's disease. *J. Comput.-Aided Mol. Des.* **2020**, *34*, 983−1002.
(71) Sinha, S. K.; Shrivastava, S. K. Synthesis, evaluation and molecular dynamics study of some new 4-aminopyridine semicarbazones as an antiamnesic and cognition enhancing agents. *Bioorg. Med. Chem.* **2013**, *21*, 5451−5460.

https://doi.org/10.1021/acsomega.2c08061
ACS Omega 2023, 8, 9394−9414